Consideration of unsolubilized matter and leachate recirculation in a two-step anaerobic digestion model: impacts on methane production

Oumaima Laraj, Noha El Khattabi, Alain Rapaport, Jérôme Harmand

Consideration of unsolubilized matter and leachate recirculation in a two-step anaerobic digestion model: impacts on methane production

Oumaima Laraj[1], Noha El Khattabi[1], Alain Rapaport[2], and Jérôme Harmand[3]

[1]Laboratory of Mathematical Analysis and Applications, Mohammed V University, Rabat, Morocco
[2]MISTEA, Univ. Montpellier, INRAE, Institut Agro, Montpellier, France
[3]LBE, INRAE, Univ. Montpellier, Narbonne, France
[1]oumaima_laraj@um5.ac.ma, noha.elkhattabi@fsr.um5.ac.ma
[2]alain.rapaport@inrae.fr
[3]jerome.harmand@inrae.fr

Abstract

In this paper, we focus on describing a landfill or a 'well-controlled' anaerobic composting area where leachate recirculation can be managed. We assume that this system can be modeled as a two-stage anaerobic digester, allowing us to analyze the biological interactions through a mathematical model that represents the dynamics of the anaerobic process. The work's originality lies in the fact that we consider different compartments of organic matter with respect to the rates at which they become accessible to the biomass for its growth, which explicitly depends on the recirculation rate. The different compartments are unsolubilized organic matter (sometimes named slowly degradable) and solubilized organic matter (rapidly degradable). The methane produced is evaluated as a function of the initial solubilized matter and the leachate recirculation rate. The study shows that when the kinetics is monotonically increasing, the ordering of solutions could be preserved subject to certain constraints on the parameters and then the methane production can be seen as an increasing function of initial solubilized matter. In addition, it is shown that the leachate recirculation rate and the initial distribution of organic matter affect methane production significantly in the presence of biomass inhibition. A numerical investigation shows that a minimum of recirculation could enhance the methane production and allow the conversion of a high initial organic load.

Keywords: Anaerobic digestion; methane; leachate recirculation; non hyperbolic equilibria; singular perturbations; solutions comparison; sensitivity.

1 Introduction

Solid waste, which contains a high organic matter content, may be treated either through aerobic or anaerobic biological pathways. Anaerobic digestion converts the biodegradable fraction of bioresources, such as lipids, proteins, and carbohydrates, into digestate (biomass) and biogas composed of a mixture of carbon dioxide and methane, a product that can be valorized as a source of energy [27]. Keeping in mind the growing demand for green energy on a global scale [28] and the availability of waste, anaerobic digestion can be used to valorize waste in landfills or composting areas. Indeed, recently, there has been an increasing interest in the commercial uses of anaerobic digestion in waste treatment facilities for its environmental and economic benefits [15]. When working with such a system, the selection of the main primary organic resource is an important aspect of the process. However, anaerobic digestion is a complex natural process involving a large number of bacterial strains [13] and is not yet fully understood.

Traditionally, landfills were seen as containment structures where waste was merely stored. However, this approach has faced criticism, particularly concerning the generation and spread of contaminated leachate capable

of polluting soils and aquifers [12]. These identified issues can be addressed through an alternative contemporary perspective, wherein landfills are considered as managed sites where solid waste undergoes treatment and stabilization. Such sites have been waterproofed to avoid the leakage of leachate. In most advanced sites, the leachate can be collected and treated or recirculated as a way of keeping a sufficiently high water content to facilitate and boost biological processes [5, 9] so that the organic component is minimized and byproducts such as biogas are generated [30]. To better understand the conditions under which the process operates effectively, we can use mathematical modeling [26, 19].

In the historical context of anaerobic digestion modeling, numerous comprehensive mathematical models were developed to understand and predict process dynamics [25, 8] and the references therein. Among these, the so-called 'ADM1' serves as a reference model developed by Batstone et al. [7]. The ADM1 is a high-dimensional model as it includes the four main stages of anaerobic decomposition: hydrolysis, acidogenesis, acetogenesis, and methanogenesis, as well as growth and decay of different biomass fractions. Additionally, physicochemical and kinetic processes are included. Due to its high complexity and strong non-linearity, ADM1 cannot be used for qualitative analysis of the system. However, when dealing with processes with a relatively high water content, there is a wide range of publications describing the successful use of ADM1 for forecasting and simulating biogas plants with a large number of different substrates and operating modes. A review of mathematical modeling of anaerobic digestion, with an emphasis on modeling for control, is provided in [19]. In most biogas installations, about 70% of methane is produced through the conversion of acetate. By focusing on this principal pathway and separating hydrolysis from the overall process, the representation of the system can be simplified into two main reactions: acidogenesis and methanization, which are described by the so-called AM2 model [10], a four-dimensional system, as modeled in [39, 22, 34, 20]. In [10], monotone growth of the bacteria was assumed, and the existence and stability properties of the equilibrium points were explored. Even though the AM2 model has proven useful for the control and monitoring of anaerobic bioreactors, it remains a very simple model, unable to describe certain biological phenomena, such as the dynamics of lower concentrations or small microorganisms [1]. Therefore, a different, more extended approach to modeling anaerobic digestion was taken in [39, 14, 20, 18] with the aim of better describing the process by integrating new main variables. In Rouez's model [39], a simplification was proposed in which the process is reduced to two fundamental steps: hydrolysis/acidogenesis and methanogenesis. This model was extended in [40] by considering that part of the dead microorganisms returns to the solubilized material. It is shown for non-monotonic growth functions that the performances in terms of biogas production are discontinuous with respect to the initial condition since the global attractor is non-connected.

The biodegradation of waste in a landfill environment is affected by several factors such as waste composition and age, operational conditions, pH, moisture content, temperature, nutrient availability, etc. [11]. However, moisture content has been determined to be the most critical parameter [46]. For instance, the main process used for controlling the moisture content of waste is leachate recirculation. It can be operated and manipulated to enhance system mixing, improve degradation, and enhance biogas generation. Several studies have assessed the impact of leachate recirculation through pilot-scale experiments [23, 41]. For example, gas production rates were found to double in wetter zones of a partially recirculating landfill compared to drier areas, while a 12-fold increase in gas production was observed in recirculating cells compared to conventional ones [38]. However, few studies have reported on the improvement of gas collection through leachate recirculation in a mathematical context, particularly in the long term in the field. There are few simple models describing anaerobic digestion that take into account a hydrolytic process [16, 2, 17]. In [36], the authors present a simple model of a landfill that describes the degradation of the soluble substrate by means of anaerobic biomass and the solubilization of the insoluble one through leachate recirculation under perfect mixing conditions.

There are many variables that affect methane production from substrates during anaerobic digestion. The most obvious one is the different substrates and proportions of substrates added. Previous models for anaerobic digestion in landfills [40, 39, 36] did not take into account the composition of the organic mixture to be treated. Thus, in this paper, we restructure the complex matter compartment by including a new variable (unsolubilized) in the model considered in [40] and taking into consideration the leachate recirculation that connects the two components via a solubilization process. This work presents a detailed mathematical analysis of the asymptotic behavior of the corresponding model and gives relevant mathematical conclusions. Moreover, it proposes a brief revisit of some qualitative results from [40] by adapting the proofs, especially to characterize the global attractor. In this study, we consider both non-solubilized and solubilized matter converted to methane in a two-stage anaerobic digestion process using a coupled model. Our main objective is to study the effects of this consideration on the system's performance. In particular, we examine under what operating conditions and leachate parameter there is a significant effect on methane production.

The paper is organized as follows. First, the model is described in detail. We give some preliminary results related to the asymptotic behavior of the solutions. Then, the qualitative analysis is presented, with the determination of the equilibrium points and the characterization of a global attractor. In section 4, we evaluate methane production depending on the leachate recirculation rate and input parameters. After reducing the model to a

three-dimensional system, we give conditions under which the vector order of solutions of this model is preserved for monotonically increasing kinetics. Finally, a numerical sensitivity investigation of the model with respect to key parameters and input values was carried out before conclusions and perspectives are formulated.

2 Model and assumptions

In landfills, the different types of organic matter present in a mix of waste are not all equal when it comes to decomposition. Some materials are very easily and therefore quickly degraded by microorganisms. Other materials, on the contrary, are called 'unsolubilized' because of their resistance to decomposition which can be enhanced by leachate recirculation in anaerobic environments [9, 5]. This recirculation is aimed in particular at reviving biological activity by adding humidity within the waste insofar as certain areas of the massif would have a lower level of water content.

In our context, we consider a simplified mathematical model of anaerobic digestion as a two-stage process in batch mode. This model, initially proposed by Rouez [39] and completely analyzed in [40] with a biomass recirculation and a generic growth law is generalized in the present work. We take into consideration the composition of the organic mixing under the influence of leachate recirculation on the hydrolysis process. Thus, we integrate a new variable (X^{u}) standing for the concentration of unsolubilized organic matter. The recirculation of leachate provided that X^{u} which is not consumed directly by the biomass is converted into a solubilized one (X^{s}). During the first stage, X^{s} is transformed into substrate (S). Methanogenic bacteria (B) then convert substrate into methane (M).

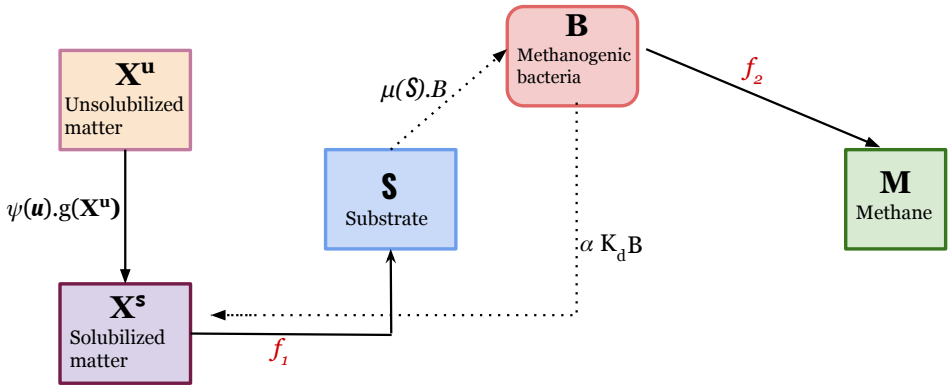

Figure 1: Overall diagram of anaerobic digestion process under the effect of leachate recirculation with an unsolubilized matter.

Let us notice that we are interested on methane only as a bioproduct. Thus, the proposed mathematical model reads as follows:

$$\begin{cases} \dot{X}^{\mathrm{u}} = -\psi(u)g(X^{\mathrm{u}}) \\ \dot{X}^{\mathrm{s}} = -K_h X^{\mathrm{s}} + \psi(u)g(X^{\mathrm{u}}) + \alpha K_d B \\ \dot{S} = f_1 K_h X^{\mathrm{s}} - \frac{1}{Y}\mu(S)B \\ \dot{B} = (\mu(S) - K_d)B \\ \dot{M} = f_2 \frac{1-Y}{Y}\mu(S)B \end{cases} \tag{1}$$

where $X_0^{\mathrm{u}}, X_0^{\mathrm{s}}, S_0, B_0$ and M_0 denote the initial concentrations of unsolubilized, solubilized organic matters, substrate, biomass and methane, respectively. The parameters $K_h, \alpha, K_d, f_1, f_2, Y$ and u are positive and constant, as given in Table 1. The kinetics μ depends only on S and the functions ψ and g are the leachate flow rate and the conversion rate of X^{u} to X^{s}, respectively. Thus, the product $\psi(u)g(X^{\mathrm{u}})$ describes the solubilization rate of unsolubilized matter into solubilized one under the effect of leachate recirculation flow rate. Variables S and B are measured in equivalent carbon mass where S is converted in B with a yield coefficient $Y < 1$. Therefore $\frac{1}{Y}$

Table 1: Parameters and assumptions.

Parameters	Significance	Assumptions
K_h	Hydrolysis rate (hours^{-1})	$K_h > 0$
K_d	Biomass mortality rate (hours^{-1})	$0 < K_d < \max_{s>0} \mu(s)$
Y	Yield substrate conversion	$Y < 1$
α	Proportion of nutrient recycling	$\alpha < 1$
u	Leachate recirculation rate (hours^{-1})	$u \in [0, +\infty)$
f_i $(i = 1, 2)$	Stoichiometric coefficients	$f_i < 1$

is larger than 1 because the remaining fraction $\frac{1}{Y} - 1 = \frac{1-Y}{Y}$ is converted into biogas with some efficiency factor f_2.

In the following, $\mathbb{R}_+$ and $\mathbb{R}_+^\star$ denote the set of non negative and positive numbers, respectively. We consider the following assumptions on the considered functions.

$\mathbf{A_1}$. $\mu : \mathbb{R}_+ \to \mathbb{R}_+$ is of class $\mathcal{C}^1$, such that $\mu(S) > 0$ for $S > 0$ with $\mu(0) = 0$.

$\mathbf{A_2}$. $\psi : \mathbb{R}_+ \to \mathbb{R}_+$ is of class $\mathcal{C}^1$ and increasing with $\psi(0) = 0$.

$\mathbf{A_3}$. $g : \mathbb{R}_+ \to \mathbb{R}_+$ is of class $\mathcal{C}^1$, increasing with $g(0) = 0$. Moreover, we assume that there exists $\nu > 0$ such that $g'(X^{\mathrm{u}}) > \nu$ for all $X^{\mathrm{u}} \geq 0$.

3 Study of the asymptotic behavior

Note that the system (1) has a cascade structure. In the mathematical analysis, we overlook the last equation, as it represents the model output. Therefore, we consider the reduced model (2) and give some analytical results of system (2) in the following section.

$$\begin{cases} \dot{X}^{\mathrm{u}} = -\psi(u) g(X^{\mathrm{u}}) \\ \dot{X}^{\mathrm{s}} = -K_h X^{\mathrm{s}} + \psi(u) g(X^{\mathrm{u}}) + \alpha K_d B \\ \dot{S} = f_1 K_h X^{\mathrm{s}} - \frac{1}{Y} \mu(S) B \\ \dot{B} = (\mu(S) - K_d) B \end{cases} \tag{2}$$

Remark 3.1. *The vector field associated to the system of equations (2) is of class $\mathcal{C}^1$ in $\mathbb{R}^4$, and thus the existence and uniqueness of solutions of (2) on a maximal time interval are guaranteed for any non-negative initial condition by the classical Cauchy Lipschitz argumentation.*

Proposition 3.1. *Assume ($\mathbf{A_1}$), ($\mathbf{A_2}$) and ($\mathbf{A_3}$) hold. Then, for any non-negative initial condition, the solution of (2) is defined for any positive time, non-negative and bounded.*

Proof. Let $(X_0^{\mathrm{u}}, X_0^{\mathrm{s}}, S_0, B_0)$ be a non-negative initial condition and consider $(X^{\mathrm{u}}, X^{\mathrm{s}}, S, B)$ the associated solution of (2).
If $B_0 = 0$, then the solution satisfies $B(t) = 0$ for any $t > 0$. If $B_0 > 0$, by uniqueness of the solution, $B(\cdot)$ cannot reach $B = 0$ in finite time. We can then deduce that $B(t)$ is non-negative for any positive t, in any case.
Furthermore, since the function $g(.)$ is of class $\mathcal{C}^1$ on $\mathbb{R}_+$ with $g(0) = 0$, using a same argument, $X^{\mathrm{u}}(.)$ remains positive, and the solution $X^{\mathrm{u}}(.)$ for $X_0^{\mathrm{u}} = 0$ is identically null. Thus, $X^{\mathrm{u}}(t) \geq 0$ for any $t > 0$.
On the other hand, one has $\dot{X}^{\mathrm{s}} \geq -K_h X^{\mathrm{s}}$, which proves the non-negativity of $X^{\mathrm{s}}(t)$ for any positive t.
Moreover, from equations (2), one has $\dot{S} \geq -\frac{1}{Y} \mu(S) B(t)$.
Let us consider the following non-autonomous scalar dynamics and denote $\tilde{S}$ its solution.

$$\begin{cases} \dot{\tilde{S}} = -\frac{1}{Y} \mu(\tilde{S}) B(t) \\ \tilde{S}(0) = S_0. \end{cases} \tag{3}$$

Since $\mu(0) = 0$, we can deduce that $\tilde{S}(t) = 0$ is solution of (3) for any $t > 0$, when $S_0 = 0$. As μ is Lipschitz continuous, we deduce by uniqueness of the solution that $\tilde{S}(\cdot)$ is positive for $S_0 > 0$. By comparison of solutions for scalar ordinary differential equations (see e.g. [45]), one has $S(t) \geq \tilde{S}(t) \geq 0$, for any $t > 0$ whatever is the non-negative initial condition.
On the other hand, we introduce the following function defined by

$$V(t) = X^{\mathfrak{u}}(t) + X^{\mathfrak{s}}(t) + \alpha(YS(t) + B(t)). \tag{4}$$

From equations (2), one has

$$\dot{V} = K_h(\alpha f_1 Y - 1)X^{\mathfrak{s}}. \tag{5}$$

Under the assumptions provided in Table 1, one has $\alpha f_1 Y < 1$ and as $X^{\mathfrak{s}}$ remains non-negative, we conclude that V is non-increasing. Thus, $0 \leq V(t) \leq X_0^{\mathfrak{u}} + X_0^{\mathfrak{s}} + \alpha(YS_0 + B_0)$, $\forall t \geq 0$. Therefore, $V(t)$ converges to a limit, which will be denoted $V^\infty \geq 0$, as t tends to $+\infty$. We deduce that $(X^{\mathfrak{u}}, X^{\mathfrak{s}}, S, B)$ is bounded. ■

We first perform an asymptotic analysis of model (2). Then, we provide a characterization of its global attractor.
Denote the state vector of model (2) by $\Sigma = [X^{\mathfrak{u}}, X^{\mathfrak{s}}, S, B]^\intercal$.

Proposition 3.2. *Let $u > 0$ and assume ($\mathbf{A_1}$), ($\mathbf{A_2}$) and ($\mathbf{A_3}$) hold. For any non-negative initial condition $\Sigma_0 = [X_0^{\mathfrak{u}}, X_0^{\mathfrak{s}}, S_0, B_0]^\intercal$, one has, for some $S_u^\infty \geq 0$*

$$\Sigma^\star := \lim_{t\to+\infty} \Sigma(t) = [0, 0, S_u^\infty, 0],$$

where $S_u^\infty \leq S_0 + \frac{X_0^{\mathfrak{u}} + X_0^{\mathfrak{s}}}{\alpha Y} + \frac{B_0}{Y}$. Moreover, if $X_0^{\mathfrak{u}} + X_0^{\mathfrak{s}} + S_0 > 0$, then S_u^∞ is non-null.

Proof. Using equations (2) and (5), one has

$$\ddot{V} = K_h(\alpha f_1 Y - 1)(-K_h X^{\mathfrak{s}} + \psi(u)g(X^{\mathfrak{u}}) + \alpha K_d B), \tag{6}$$

from which, under assumptions ($\mathbf{A2}$) and ($\mathbf{A_3}$), we deduce that $\ddot{V}$ is bounded and thus $\dot{V}$ is uniformly continuous on $\mathbb{R}_+$. Then, one can get from Barbalat's Lemma [4] that $\lim_{t\to+\infty} \dot{V}(t) = 0$ which implies from (5) that

$$\lim_{t\to+\infty} X^{\mathfrak{s}}(t) = 0. \tag{7}$$

Moreover, one has

$$\ddot{X}^{\mathfrak{u}} + \ddot{X}^{\mathfrak{s}} = -K_h(-K_h X^{\mathfrak{s}} + \psi(u)g(X^{\mathfrak{u}})) + \alpha K_d B(\mu(S) - K_d - K_h).$$

Similarly, as $\dot{X}^{\mathfrak{u}} + \dot{X}^{\mathfrak{s}}$ is uniformly continuous on $\mathbb{R}_+$, Barbalat's Lemma [4] implies that $\lim_{t\to+\infty} [\dot{X}^{\mathfrak{u}}(t) + \dot{X}^{\mathfrak{s}}(t)] = 0$.
From (7), we deduce that $\lim_{t\to+\infty} B(t) = 0$.
In addition, one has

$$\ddot{X}^{\mathfrak{u}} = (\psi(u))^2 g'(X^{\mathfrak{u}})g(X^{\mathfrak{u}}).$$

As $u > 0$ and from ($\mathbf{A_3}$), we obtain using the same arguments $\lim_{t\to+\infty} X^{\mathfrak{u}}(t) = 0$. Finally, from (4) one can deduce that there exists

$$S_u^\infty \in \mathbb{R}_+, \lim_{t\to+\infty} S(t) = S_u^\infty = \frac{V^\infty}{\alpha Y}.$$

On the other hand, one has

$$S_u^\infty \leq S_0 + \frac{X_0^{\mathfrak{u}} + X_0^{\mathfrak{s}}}{\alpha Y} + \frac{B_0}{Y}.$$

Now let us show that $S_u^\infty \neq 0$ when $X_0^{\mathfrak{u}} + X_0^{\mathfrak{s}} > 0$ or $S_0 > 0$.
Suppose that $S_u^\infty = 0$, then by continuity of $\mu(.)$ and as $\mu(0) = 0$, one has

$$\lim_{t\to+\infty} \mu(S(t)) = 0$$

which implies that there exists $T > 0$ such that

$$\mu(S(t)) \leq \alpha f_1 Y K_d, \quad \forall t \geq T. \tag{8}$$

In addition, one obtains from the first three equations of (2)

$$f_1(\dot{X}^{\mathfrak{u}} + \dot{X}^{\mathfrak{s}}) + \dot{S} = \frac{1}{Y}(\alpha f_1 Y K_d - \mu(S))B. \tag{9}$$

Thus, from (8) we get $f_1(\dot{X}^{\mathfrak{u}}(t)+\dot{X}^{\mathfrak{s}}(t))+\dot{S}(t)\geq 0$, for any $t\geq T$.
On the other hand, it has been shown previously that the variables $X^{\mathfrak{u}}(.)+X^{\mathfrak{s}}(.)$ or $S(.)$ are positive when $X_0^{\mathfrak{u}}+X_0^{\mathfrak{s}}>0$ or $S_0>0$. Since $f_1(X_0^{\mathfrak{u}}+X_0^{\mathfrak{s}})+S_0>0$, we deduce that $f_1(X^{\mathfrak{u}}+X^{\mathfrak{s}})+S$ cannot reach 0 in finite time. One has then

$$f_1(X^{\mathfrak{u}}(t)+X^{\mathfrak{s}}(t))+S(t)\geq f_1(X^{\mathfrak{u}}(T)+X^{\mathfrak{s}}(T))+S(T)>0,\quad t\geq T,$$

and

$$\lim_{t\to+\infty}[f_1(X^{\mathfrak{u}}(t)+X^{\mathfrak{s}}(t))+S(t)]>0,$$

which is in contradiction with the fact that $S_u^{\infty}=0$ and $\lim_{t\to+\infty}[X^{\mathfrak{u}}(t)+X^{\mathfrak{s}}(t)]=0$. Thus, we conclude our result. ■

Remark 3.2. *In the case of no recirculation ($u=0$), we have $\lim_{t\to+\infty}X^{\mathfrak{u}}(t)=X_0^{\mathfrak{u}}$. Then, from (4), one has*

$$S^{\infty}:=S_{u=0}^{\infty}=\frac{V^{\infty}-X_0^{\mathfrak{u}}}{\alpha Y}$$

and as $X^{\mathfrak{u}}$ is constant, S^{∞} is independent of $X_0^{\mathfrak{u}}$ as expected (the dynamics $X^{\mathfrak{u}}$ is decoupled with $u=0$).

The model (2) admits a continuum of equilibria. Moreover, one can check that one of the eigenvalues of the Jacobian matrix at these equilibrium points is always zero, implying that all equilibria of (2) are non hyperbolic. Consequently, classical stability analysis techniques for hyperbolic equilibria cannot be applied. To overcome this limitation, we employ an alternative approach: we represent the solutions of the original non-hyperbolic system as solutions of a family of hyperbolic systems, then apply the stable manifold theory and demonstrate the exponential convergence of the corresponding trajectories. The characterization of the set of equilibria that can be reached by positive solutions and the global attractor are given below in Propositions 3.3 and 3.4.

Before characterizing the global attractor of the system (2), let us introduce the following result concerning the set of equilibria points towards which solutions converge. We define the set

$$\mathcal{E}:=\{S\in\mathbb{R}_+:\mu(S)\leq K_d\}. \tag{10}$$

Proposition 3.3. *Assume ($\mathbf{A_1}$), ($\mathbf{A_2}$) and ($\mathbf{A_3}$) hold. For an initial condition in $\mathbb{R}_+^4$ with $X_0^{\mathfrak{u}}+X_0^{\mathfrak{s}}>0$ and $B_0>0$, the solution of (2) converges asymptotically to an equilibrium $\Sigma^{\star}=(0,0,S_u^{\infty},0)$ with $S_u^{\infty}\in\mathcal{E}\setminus\{0\}$.*

Proof. If $S_u^{\infty}\notin\mathcal{E}$, for t sufficiently large, one gets

$$(\mu(S(t))-K_d)>\epsilon:=\frac{\mu(S_u^{\infty})-K_d}{2}.$$

Consequently, and since $B(.)$ is non-negative, we obtain for t sufficiently large

$$\dot{B}(t)>\epsilon B(t).$$

By a standard comparison theorem for differential inequalities [45], one gets

$$B(t)>B(\tau)e^{\epsilon(t-\tau)}\quad \text{for t,}\tau\text{ sufficiently large s.t } t\geq\tau.$$

We deduce that $B(.)$ cannot converge asymptotically to 0, which is in contradiction with the result obtained in Proposition 3.2. ■

As the model (2) is a generalized version of the model introduced in [40], we revisit it by adapting the proof given in this reference to show that the attractor of (2) is characterized in the following result.

Proposition 3.4.

$$\mathcal{A}:=\{0\}\times\{0\}\times\mathcal{E}\times\{0\}$$

is a forward attractor for any non-negative initial condition of the dynamics (2).

Proof. To prove this proposition, we introduce a change of variable Z to replace S for a given fixed initial condition, which will represent the solution of (2) as a solution of a system where 0 is an hyperbolic equilibrium. This will allow us to use the stable manifold theorem. Then, we obtain that trajectory corresponding to the chosen initial condition belongs to the stable manifold of the equilibrium of this system with the Z variable and thus converges exponentially to 0.

Let us fix $\Sigma^\star = (0, 0, S_u^\infty, 0)$ such that $S_u^\infty > 0$ and $\mu(S_u^\infty) < K_d$. For solutions with $B(t) > 0$, consider the variable $Z(.)$ defined by

$$Z(t) = \frac{f_1(X^u(t) + X^s(t)) + (S(t) - S_u^\infty)}{B(t)} + \beta, \quad \forall t \geq 0$$

where

$$\beta = \frac{\frac{1}{Y}\mu(S_u^\infty) - \alpha f_1 K_d}{\mu(S_u^\infty) - K_d}.$$

Note that this change of coordinates depends on the asymptotic value of S and thus of the initial condition. By a direct computation, we obtain

$$\dot{Z}(t) = -\gamma(\mu(S) - \mu(S_u^\infty)) - (\mu(S) - K_d)Z(t)$$

with

$$\gamma = \frac{K_d(1 - \alpha f_1 Y)}{Y(K_d - \mu(S_u^\infty))} > 0.$$

We consider the domain

$$\mathcal{K} = \{(X^u, X^s, Z, B) \in \mathbb{R}_+^2 \times \mathbb{R} \times \mathbb{R}_+^\star / S_u^\infty - f_1(X^u + X^s) + (Z - \beta)B \geq 0\}.$$

We can rewrite the system (2) in terms of X^u, X^s, Z and B on the domain $\mathcal{K}$ as follows

$$\begin{cases} \dot{Z} = -\gamma(k(Z, X^u, X^s, B) - \mu(S_u^\infty)) - (k(Z, X^u, X^s, B) - K_d)Z \\ \dot{X}^u = -\psi(u)g(X^u) \\ \dot{X}^s = -K_h X^s + \psi(u)g(X^u) + \alpha K_d B \\ \dot{B} = (k(Z, X^u, X^s, B) - K_d)B \end{cases} \tag{11}$$

with

$$k(Z, X^u, X^s, B) = \mu(S_u^\infty - f_1(X^u + X^s) + (Z - \beta)B).$$

It's easy to see that the region $\mathcal{K}$ is positively invariant for (11). Furthermore, the dynamics (11) is well defined for $B = 0$ and regular on the set $\bar{\mathcal{K}}$ which is also positively invariant. Any trajectory of (11) in $\mathcal{K}$ matches a trajectory of (2) where

$$S(t) = S_u^\infty - f_1(X^u(t) + X^s(t)) + (Z(t) - \beta)B(t), \quad \forall t \geq 0.$$

However, we can observe that trajectories of (11) with $B(.) = 0$ does not necessarily match a trajectory of (2). By reminding that $\mu(S_u^\infty) \neq K_d$, we can check that the origin is the unique equilibrium of (11) in $\bar{\mathcal{K}}$.
The linearization of (11) near the origin is based on the following Jacobian matrix

$$J = \begin{pmatrix} -(\mu(S_u^\infty) - K_d) & \gamma f_1 \mu'(S_u^\infty) & \gamma f_1 \mu'(S_u^\infty) & \gamma\beta\mu'(S_u^\infty) \\ 0 & -\psi(u)g'(0) & 0 & 0 \\ 0 & \psi(u)g'(0) & -K_h & \alpha K_d \\ 0 & 0 & 0 & \mu(S_u^\infty) - K_d \end{pmatrix}.$$

Under the condition $\mu(S_u^\infty) < K_d$, J has eigenvalues whose real parts are different from 0: $-K_h$, $-\psi(u)g'(0)$, $\mu(S_u^\infty) - K_d$ and $-(\mu(S_u^\infty) - K_d)$.
Since the origin is an hyperbolic equilibrium, then from the Stable Manifold Theorem [32], there exist a three-dimensional stable manifold $W^s(0)$ and a one unstable manifold $W^u(0)$ for the origin. It's clear that $W^u(0) = \{0\} \times \{0\} \times \mathbb{R} \times \{0\}$.
On the other hand, let us show that any point $(Z, X^u, X^s, B) \in W^s(0) \setminus (0, 0, 0, 0)$ has to be such that $B \neq 0$.
If $B_0 = 0$, any solution of (11) verifies $B(t) = 0$, $\forall t > 0$. Moreover, since both $X^u(t)$ and $X^s(t)$ converge to 0 when t tends to $+\infty$, it implies that

$$\lim_{t \to +\infty} k(Z(t), X^u(t), X^s(t), B(t)) = \mu(S_u^\infty), \text{whatever is } Z(0).$$

Consequently, for any $Z(0), X_0^u, X_0^s$ and for t sufficiently large, one has

$$K_d - k(Z(t), X^u(t), X^s(t), B(t)) > \frac{1}{2}(K_d - \mu(S_u^\infty)),$$

then $\lim_{t\longrightarrow+\infty} Z(t) = +\infty$. It can be deduced from this that any point $(Z, X^{\mathfrak{u}}, X^{\mathfrak{s}}, B) \in W^s(0) \setminus (0,0,0,0)$ has to be such that $B \neq 0$. We deduce that any trajectory of (11) in $W^s(0) \cap \mathcal{K}$ corresponds to a trajectory of (2) and converges asymptotically to 0. Finally, we can say that for any equilibrium point $\Sigma^\star$ with $S_u^\infty \in int\ \mathcal{E}$, there exists a three-dimensional invariant manifold $W^s(0) \cap \mathcal{K}$ in $\mathbb{R}^4_+$, such that all solutions of (2) with an initial condition in $W^s(0) \cap \mathcal{K}$ converge asymptotically to $\Sigma^\star$. With the convergence of solutions of (2) towards an equilibrium that belongs to $\mathcal{E}$, as stated in Proposition 3.3, our result is proved. ■

Remark 3.3. *For non-monotonic growth functions, the set $\mathcal{E}$ is not connected, as an union of disjoint intervals $\mathcal{E} = I_1 \cup I_2 \cup \cdots$. Therefore, the global attractor $\mathcal{A}$ of the dynamics (2) is non-connected.*

For a given initial condition $(X_0^{\mathfrak{u}}, X_0^{\mathfrak{s}}, S_0, B_0, 0)$, we consider the final production of methane, that is the asymptotic value of the variable M in (1), as a function of the recirculation rate u, that we denote by M_u^∞.

Proposition 3.5. *Assume (**A1**), (**A2**) and (**A3**) hold. For any non-negative initial condition $(X_0^{\mathfrak{u}}, X_0^{\mathfrak{s}}, S_0, B_0, 0)$ and recirculation rate u, the methane produced in system (1) is given by the following expression*

$$M_u^\infty = \begin{cases} \dfrac{f_1(X_0^{\mathfrak{u}} + X_0^{\mathfrak{s}}) + \alpha f_1 B_0 + (S_0 - S_u^\infty)}{a_1} & \text{if } u > 0 \\ \dfrac{f_1 X_0^{\mathfrak{s}} + \alpha f_1 B_0 + (S_0 - S^\infty)}{a_1} & \text{if } u = 0 \end{cases} \tag{12}$$

where $a_1 = \frac{1-\alpha Y f_1}{f_2(1-Y)}$ is a positive number and the existence of S_u^∞ and S^∞ are given by Proposition 3.2 and Remark 3.2.

Proof. Since $V(.)$ is bounded in (4), then $\int_0^t X^{\mathfrak{s}}(z)dz < +\infty$. Moreover, by integrating eqs. (1) between $t = 0$ and $t = +\infty$, one gets the following system of two linear equations for any positive u

$$\begin{cases} K_h \int_0^\infty X^{\mathfrak{s}}(z)dz - \alpha \int_0^\infty \mu(S(z))B(z)dz = X_0^{\mathfrak{u}} + X_0^{\mathfrak{s}} + \alpha B_0 \\ f_1 K_h \int_0^\infty X^{\mathfrak{s}}(z)dz - \frac{1}{Y} \int_0^\infty \mu(S(z))B(z)dz = S_u^\infty - S_0 \end{cases} \tag{13}$$

whose solution is unique, well defined under the condition $1 - \alpha Y f_1 > 0$, and given by the expressions

$$\int_0^\infty X^{\mathfrak{s}}(z)dz = \frac{(X_0^{\mathfrak{u}} + X_0^{\mathfrak{s}}) + \alpha B_0 + \alpha Y(S_0 - S_u^\infty)}{K_h(1 - \alpha f_1 Y)}$$

$$\int_0^\infty \mu(S(z))B(z)dz = Y \frac{(S_0 - S_u^\infty) + f_1(X_0^{\mathfrak{u}} + X_0^{\mathfrak{s}}) + \alpha f_1 B_0}{1 - \alpha f_1 Y}.$$

Thus, one obtains

$$M_u^\infty = f_2(1 - Y) \frac{f_1(X_0^{\mathfrak{u}} + X_0^{\mathfrak{s}}) + \alpha f_1 B_0 + (S_0 - S_u^\infty)}{1 - \alpha f_1 Y}.$$

On the other hand, if $u = 0$, since $\lim_{t\to+\infty} X^{\mathfrak{u}}(t) = X_0^{\mathfrak{u}}$ and using Remark 3.2, the system (13) becomes

$$\begin{cases} K_h \int_0^\infty X^{\mathfrak{s}}(z)dz - \alpha \int_0^\infty \mu(S(z))B(z)dz = X_0^{\mathfrak{s}} + \alpha B_0 \\ f_1 K_h \int_0^\infty X^{\mathfrak{s}}(z)dz - \frac{1}{Y} \int_0^\infty \mu(S(z))B(z)dz = S^\infty - S_0. \end{cases} \tag{14}$$

Therefore, the methane produced in the case of no recirculation is given by the following expression

$$M_u^\infty = f_2(1 - Y) \frac{f_1 X_0^{\mathfrak{s}} + \alpha f_1 B_0 + (S_0 - S^\infty)}{1 - \alpha f_1 Y}.$$

This ends the proof. ■

4 Influence of leachate recirculation and initial conditions on methane production

Methane production is a crucial component of waste management, particularly in landfill operations where anaerobic digestion is a key process. This methane can be harnessed as a green energy source by combusting it to generate combined heat and power, using it as vehicle fuel, or injecting it into the natural gas grid [35]. Optimizing methane generation and minimizing its environmental impact requires a good understanding of the influencing factors. Among these, leachate recirculation rate, represented by the parameter u, plays a significant role as it modify the asymptotic value of S. Additionally, initial conditions, including the initial microbial concentration and substrate availability, can significantly affect the overall performance and dynamics of methane production. This section investigates the influence of both leachate recirculation and initial conditions on asymptotic methane production.

4.1 Influence of leachate recirculation rate

From Proposition 3.5, it is important to note that M_u^∞ depends on S_u^∞, which varies with the recirculation parameter u. For $u > 0$, the asymptotic value S_u^∞ depends on both initial X_0^{u} and X_0^{s}, while for $u = 0$, it does not depend on X_0^{u} (cf Remark 3.2). This suggests that the map $u \mapsto M_u^\infty$ might be discontinuous at $u = 0$, and thus motivates the analysis of its continuity properties.

4.1.1 Dependency with respect to the recirculation rate

In the following result, we show that the function associating the recirculation rate u with the asymptotic methane production M_u^∞ is lower semi-continuous. This mathematical property indicates that small increases in u will not cause a sudden drop in asymptotic methane, ensuring that the methane production does not experience abrupt decreases as the recirculation rate is adjusted.

Proposition 4.1. *For any non-negative initial condition $(X_0^{\mathrm{u}}, X_0^{\mathrm{s}}, S_0, B_0, 0)$, the map $u \in \mathbb{R}_+ \mapsto M_u^\infty$ is lower semi-continuous.*

Proof. Fix $u \geq 0$ and a number $\epsilon > 0$. Let us denote by $M_u(t)$ the solution $M(t)$ in system (1). As $M_u(\cdot)$ is an increasing function converging to M_u^∞, there exists $T > 0$ such that

$$M_u(t) > M_u^\infty - \frac{\epsilon}{2}, \quad t \geq T.$$

For this fixed T, the map $v \mapsto M_v(T)$ is continuous at $v = u$, by the Theorem of continuous dependency of the solution of ordinary differential equations with respect to parameters [24]. Then, there exists $\eta > 0$ such that

$$|v - u| < \eta \;\Rightarrow\; M_v(T) > M_u(T) - \frac{\epsilon}{2}$$

and thus one has

$$|v - u| < \eta \;\Rightarrow\; M_v^\infty > M_v(T) > M_u^\infty - \epsilon$$

which implies

$$\liminf_{v \to u} M_v^\infty > M_u^\infty - \epsilon$$

and as ϵ is arbitrary, one gets

$$\liminf_{v \to u} M_v^\infty \geq M_u^\infty$$

i.e. $u \mapsto M_u$ is lower semi-continuous at any u. ∎

4.1.2 Methane production for arbitrarily large leachate recirculation rate

By employing a singular perturbation approach, we have approximated the methane production for infinite recirculation rate both over a finite and an infinite horizon. Our findings indicate that increasing the recirculation rate to arbitrarily large values does not enhance methane production.

First, let us denote X the concentration of the total organic matter that is the total of the unsolubilized and the solubilized compartments, thus, $X = X^{\mathrm{u}} + X^{\mathrm{s}}$.
If u is very large, the unsolubilized matter X^{u} varies at a fast time scale $\tau := t/\epsilon$ under the effect of leachate recirculation, while organic mixing X, substrate S, biomass B and methane M evolve at a slow time scale, with $\epsilon = \frac{1}{\psi(u)} << 1$ being a small dimensionless non-negative parameter.
Thus, the model (1) has the structure of singular perturbation

$$\begin{cases} \varepsilon \frac{dX^{\mathrm{u}}}{dt} = -g(X^{\mathrm{u}}) \\ \frac{dX}{dt} = -K_h(X - X^{\mathrm{u}}) + \alpha K_d B \\ \frac{dS}{dt} = f_1 K_h(X - X^{\mathrm{u}}) - \frac{1}{Y}\mu(S)B \\ \frac{dB}{dt} = (\mu(S) - K_d)B \\ \frac{dM}{dt} = f_2 \frac{1-Y}{Y}\mu(S)B. \end{cases} \tag{15}$$

For each fixed $u > 0$, or equivalently for each $\varepsilon = 1/\psi(u)$ fixed, let us denote $M^\infty(\epsilon) = M_u^\infty$ where M_u^∞ is given by (12).

The reduced model attached to model (15) is obtained with the singular perturbation method (see e.g. [24]). Here, the fast subsystem is

$$\frac{dX^{\mathrm{u}}}{d\tau} = -g(X^{\mathrm{u}}) \tag{16}$$

which has the single equilibrium $X^{\mathrm{u}} = 0$. The fast manifold is thus the hyperplane $X^{\mathrm{u}} = 0$, and the reduced model is obtained by substituting $X^{\mathrm{u}} = 0$ and $\epsilon = 0$ in the equations of the full model (15), that is

$$\begin{cases} \frac{dX}{dt} = -K_h X + \alpha K_d B \\ \frac{dS}{dt} = f_1 K_h X - \frac{1}{Y}\mu(S)B \\ \frac{dB}{dt} = (\mu(S) - K_d)B \\ \frac{dM}{dt} = f_2 \frac{1-Y}{Y}\mu(S)B. \end{cases} \tag{17}$$

For a given $\varepsilon > 0$, let us denote by $(X^{\mathrm{u}}(t,\varepsilon), X(t,\varepsilon), S(t,\varepsilon), B(t,\varepsilon), M(t,\varepsilon))$ the solution of (15) for a non-negative initial condition $(X_0^u, X_0, S_0, B_0, 0)$, and by $(\overline{X}(t), \overline{S}(t), \overline{B}(t), \overline{M}(t))$ the solution of the reduced system (17) for the initial condition $(X_0, S_0, B_0, 0)$.
Notice that the system (17) corresponds to the dynamics introduced by Ouchtout et al. [40] which describes the anaerobic digestion of a complex organic matter without taking into consideration a leachate recirculation phenomenon and that the solutions of (17) are exactly the solutions of (15) for the initial condition $(0, X_0, S_0, B_0, 0)$. Therefore, one has for any $\varepsilon > 0$

$$\lim_{t\longrightarrow+\infty} \overline{M}(t) = \lim_{t\longrightarrow+\infty} M(t,\varepsilon), \quad \text{for the initial condition } (0, X_0, S_0, B_0)$$

and thus there exists

$$\overline{M}^{\infty} := \lim_{t\longrightarrow+\infty} \overline{M}(t) = \frac{f_1 X_0 + \alpha f_1 B_0 + (S_0 - S_u^{\infty})}{a_1}. \tag{18}$$

We first compare the methane production predicted by the reduced model (17) with that predicted by (15) over a finite time horizon. This comparison will help to estimate the asymptotic methane produced in the two models when u is relatively large.

Lemma 4.1. *Assume* $(\mathbf{A_1})$, $(\mathbf{A_2})$ *and* $(\mathbf{A_3})$ *hold. For each fixed* T *and for any non-negative vector* $(X_0^{\mathrm{u}}, X_0, S_0, B_0, 0)$, *one has*

$$M(t,\varepsilon) - \overline{M}(t) = O(\varepsilon)$$

uniformly over the finite time interval $[0, T]$.

Proof. Let us fix a positive number T. Since

- the dynamics (15), (17) are of class $\mathcal{C}_1$ (Assumptions $(\mathbf{A_1})$, $(\mathbf{A_2})$ and $(\mathbf{A_3})$),
- the reduced problem (17) has a unique non-negative and bounded solution,
- the boundary-layer dynamics

$$\frac{dX^{\mathrm{u}}}{d\tau} = -g(X^{\mathrm{u}})$$

has 0 as the unique exponentially stable equilibrium uniformly in (X, S, B, M) (from Assumption $(\mathbf{A_3})$),

one can apply the Tikhonov's Theorem (see, for instance, [24]) which states that there exists a positive constant $\varepsilon^\star$ s.t, for all $0 < \varepsilon < \varepsilon^\star$, the singular perturbed system (15) has a unique solution and $M(t,\varepsilon) - \overline{M}(t) = O(\varepsilon)$ holds uniformly for $t \in [0, T]$. ■

We now demonstrate that when the recirculation parameter u goes to $+\infty$, the asymptotic methane production is identical for both models (15) and (17), indicating no long-term influence of u.

Proposition 4.2. *Assume* $(\mathbf{A_1})$, $(\mathbf{A_2})$ *and* $(\mathbf{A_3})$ *hold. For any non-negative vector* $(X_0^{\mathrm{u}}, X_0, S_0, B_0, 0)$, *one has*

$$\lim_{\varepsilon>0\to 0} M^{\infty}(\epsilon) = \overline{M}^{\infty}.$$

Proof. Let us fix $\eta > 0$ and consider an increasing sequence of positive numbers $T_n, n \in \mathbb{N}$, that tends to $+\infty$. Accordingly to Lemma 4.1, for each $n \in \mathbb{N}$, there exists $\varepsilon_n^\star > 0$ such that for $\varepsilon \in (0, \varepsilon_n^\star)$ one has

$$|M(T_n,\varepsilon) - \overline{M}(T_n)| < \frac{\eta}{3}\ .$$

We consider a sequence $\varepsilon_n \in (0, \varepsilon_n^\star), n \in \mathbb{N}$, such that $\lim_{n\longrightarrow+\infty} \varepsilon_n = 0$. On the other hand, when T_n tends to $+\infty$, $M(T_n, \varepsilon_n)$, $\overline{M}(T_n)$ converge to $M^{\infty}(\varepsilon_n)$, $\overline{M}^{\infty}$, respectively. Then, there exists $N \in \mathbb{N}$ such that

$$|M(T_n,\varepsilon_n) - M^{\infty}(\varepsilon_n)| < \eta/3, \quad |\overline{M}(T_n) - \overline{M}^{\infty}| < \eta/3, \quad n > N\ .$$

One obtains

$$|M^{\infty}(\varepsilon_n) - \overline{M}^{\infty}| \leq |M^{\infty}(\varepsilon_n) - M(T_n, \varepsilon_n)| + |M(T_n, \varepsilon_n) - \overline{M}(T_n)| + |\overline{M}(T_n) - \overline{M}^{\infty}| < \eta$$

which gives when n tends to $+\infty$

$$\lim_{\varepsilon > 0 \to 0} |M^{\infty}(\varepsilon) - \overline{M}^{\infty}| \leq \eta$$

and as $\eta > 0$ is arbitrarily, one gets the conclusion. ■

4.2 Influence of initial condition

In this section, the specific growth rate $\mu(.)$ is assumed to be an increasing function of substrate. We demonstrate that increasing initial organic matter $X_0^{\mathfrak{s}}$ alone, enhances methane production for any value of u.
For simplicity, we'll choose

$$\psi(u) = u \quad \text{for any } u, \quad \text{and} \quad g(X^{\mathfrak{u}}) = X^{\mathfrak{u}} \quad \text{for any } X^{\mathfrak{u}}.$$

The development for other functions is analogous and is left to the reader. The solution of the first eq. of (2) is then $X^{\mathfrak{u}}(t) = X_0^{\mathfrak{u}} e^{-ut}$. Consequently, the model (2) can be reduced to the following non-autonomous model of three equations

$$\begin{cases} \dot{X}^{\mathfrak{s}} = -K_h X^{\mathfrak{s}} + \alpha K_d B + u X_0^{\mathfrak{u}} e^{-ut} \\ \dot{S} = f_1 K_h X^{\mathfrak{s}} - \frac{1}{Y}\mu(S) B \\ \dot{B} = (\mu(S) - K_d) B. \end{cases} \tag{19}$$

This system is clearly non cooperative i.e. Kamke's condition [21] is not fulfilled on $\mathbb{R}^3_+$. However, we show that under certain assumptions when increasing initial conditions, the corresponding solutions are ordered in $X^{\mathfrak{s}}$ and B while not necessarily in S.
For convenience, let us consider the linear change of variables

$$Z = B + YS,$$

under which the dynamics (19) can be rewritten as a three-dimensional system

$$\begin{cases} \dot{X}^{\mathfrak{s}} = -K_h X^{\mathfrak{s}} + \alpha K_d B + u X_0^{\mathfrak{u}} e^{-ut} \\ \dot{Z} = Y f_1 K_h X^{\mathfrak{s}} - K_d B \\ \dot{B} = (\mu(\frac{Z-B}{Y}) - K_d) B, \end{cases} \tag{20}$$

defined on the domain

$$\mathcal{D} := \{(X^{\mathfrak{s}}, Z, B) \in \mathbb{R}^3_+ \text{ with } Z \geq B\}.$$

One can straightforwardly check that $\mathcal{D}$ is forwardly invariant by the dynamics (20) and notice that the system (20) is not cooperative either. However, we shall derive conditions to preserve the usual vector order of solutions but for a subset of initial conditions in $\mathcal{D}$, following the technique introduced in [37]. This will allow us to establish a property of methane production as a function of the initial organic solubilized matter $X_0^{\mathfrak{s}}$. To achieve this purpose, we isolate terms that prevent the system (20) to be cooperative and rewrite the system as follows:

$$\begin{cases} \dot{X}^{\mathfrak{s}} = -K_h X^{\mathfrak{s}} + \alpha K_d B + u X_0^{\mathfrak{u}} e^{-ut} \\ \dot{Z} = H(\xi) - K_d Z \\ \dot{B} = (\mu(\frac{Z-B}{Y}) - K_d) B \end{cases} \tag{21}$$

where H is the linear function

$$H(\xi) := H(X^{\mathfrak{s}}, Z, B) = Y f_1 K_h X^{\mathfrak{s}} + K_d(Z - B) = v.\xi$$

with

$$v = [Y f_1 K_h, K_d, -K_d]^{\intercal}.$$

Consider the partial order $\succeq$ on $\mathbb{R}^3_+$ defined by the cone

$$\xi_2 \succeq \xi_1 \iff \xi_2 - \xi_1 \geq 0 \quad \text{and} \quad v.(\xi_2 - \xi_1) \geq 0 \quad \text{(component wise)}.$$

We give now conditions for which the partial order $\succeq$ defined above is preserved by solutions of system (21).

Lemma 4.2. *Let $\bar{\xi}_0$, $\xi_0 \in \mathcal{D}$ be such that $\bar{\xi}_0 \succeq \xi_0$ and $Z_0 - B_0 < Y\mu^{-1}(\alpha Y f_1 K_h)$. Denote by $\bar{\xi}$ and ξ the corresponding solutions of (20) for the initial conditions $\bar{\xi}_0$ and ξ_0 respectively. If $K_d \geq K_h$, then there exists $T > 0$ such that*

$$\bar{\xi}(t) \succeq \xi(t), \quad \forall t \in [0, T].$$

Proof. Following [37], we rewrite the dynamics as a non-autonomous dynamical system

$$\dot{\xi} := \begin{bmatrix} \dot{X}^{\mathfrak{s}} \\ \dot{Z} \\ \dot{B} \end{bmatrix} = \tilde{F}(\xi) + \Phi(t) := \begin{bmatrix} -K_h X^{\mathfrak{s}} + \alpha K_d B \\ -K_d Z \\ (\mu(\frac{Z-B}{Y}) - K_d)B \end{bmatrix} + \begin{bmatrix} uX_0^{\mathfrak{u}} e^{-ut} \\ H(\xi(t)) \\ 0 \end{bmatrix}, \tag{22}$$

where $\Phi(\cdot) : \mathbb{R}_+ \mapsto H(\mathcal{D})$ is a non-negative map. We first remark that the formulation (22) is in a separate form in the sense that the autonomous part $\tilde{F}(\xi)$ is separated from the non-autonomous one $\Phi(t)$. Furthermore, one can straightforwardly check that the domain $\mathcal{D}$ is forwardly invariant for any non-negative map $\Phi(\cdot)$ and that the non-autonomous system (22) is cooperative on $\mathcal{D}$ and monotone with respect to Φ. Moreover, the gradient of H is always non null.
We use now the results of Corollary 1 of [37] for this separated form: one has to check that the conditions

i. $\frac{\partial H}{\partial Z}(X^{\mathfrak{s}}, Z, B) \geq 0$ for any $(X^{\mathfrak{s}}, Z, B) \in \mathcal{D}$,
ii. $\tilde{D}(\xi, \bar{\xi}) := v \cdot (\tilde{F}(\bar{\xi}) - \tilde{F}(\xi)) \geq 0, \quad \forall \bar{\xi}, \xi$ in $\mathcal{D}$ s.t. $\bar{\xi} \geq \xi$ and $v.(\bar{\xi} - \xi) = 0$,

are fulfilled to ensure that the partial order $\succeq$ is preserved by the solutions of (20).
As H is linear, one has $\frac{\partial H}{\partial Z} = K_d > 0$. By a direct computation, one obtains, for $\bar{\xi}, \xi$ in $\mathcal{D}$ with $\bar{\xi} \geq \xi$ and $v.(\bar{\xi} - \xi) = 0$,

$$\begin{aligned} \tilde{D}(\xi, \bar{\xi}) = &-Y f_1 K_h^2 (\bar{X}^{\mathfrak{s}} - X^{\mathfrak{s}}) + \alpha Y f_1 K_h K_d (\bar{B} - B) - K_d^2 (\bar{Z} - Z) + K_d^2 (\bar{B} - B) \\ &- K_d \mu(\frac{\bar{Z} - \bar{B}}{Y})\bar{B} + K_d \mu(\frac{Z - B}{Y})B. \end{aligned}$$

In addition, from the fact that $Y f_1 K_h (\bar{X}^{\mathfrak{s}} - X^{\mathfrak{s}}) = -K_d(\bar{Z} - Z - (\bar{B} - B))$, one writes

$$\begin{aligned} \tilde{D}(\xi, \bar{\xi}) = &Y f_1 K_h (K_d - K_h)(\bar{X}^{\mathfrak{s}} - X^{\mathfrak{s}}) + \alpha Y f_1 K_h K_d (\bar{B} - B) \\ &- K_d(\mu(\frac{\bar{Z} - \bar{B}}{Y})\bar{B} - \mu(\frac{Z - B}{Y})B). \end{aligned}$$

Since $\bar{Z} - \bar{B} = Z - B - Y f_1 K_h / K_d (\bar{X}^{\mathfrak{s}} - X^{\mathfrak{s}})$, we get $\bar{Z} - \bar{B} < Z - B$ and

$$\tilde{D}(\xi, \bar{\xi}) \geq Y f_1 K_h (K_d - K_h)(\bar{X}^{\mathfrak{s}} - X^{\mathfrak{s}}) + K_d (Y f_1 K_h \alpha - \mu(\frac{Z - B}{Y}))(\bar{B} - B).$$

As $\mu(.)$ is continuous increasing and the data satisfy the inequalities

$$\alpha Y f_1 K_h > \mu(\frac{Z_0 - B_0}{Y}) \quad \text{and} \quad K_d \geq K_h,$$

there exists $T > 0$ such that $\mu(\frac{Z(T) - B(T)}{Y}) = \alpha Y f_1 K_h \geq \mu(\frac{Z(t) - B(t)}{Y}), \forall t \in [0, T]$ and then $\tilde{D}(\xi(t), \bar{\xi}(t)) \geq 0$ for any $t \in [0, T]$.
Thus, under these conditions, having $\bar{\xi_0} \succeq \xi_0$ in $\mathcal{D}$ implies that

$$\exists T > 0 \ : \bar{\xi}(t) \succeq \xi(t), \quad \forall t \in [0, T].$$

■

Remark 4.3. *One could have alternatively checked the conditions introduced in [44] to prove that the dynamics is monotone with respect to the cone associated to $\succeq$. It turns out that computation is less easy than with the formulation proposed in [37].*

From Lemma 4.2, we can easily deduce the following result which shows that increasing the amount of initial organic matter only, results in a higher production of methane.
Let us denote M_t the methane produced in (19) on the time interval from 0 to t which is expressed as follows

$$M_t := M(t) = f_2 \frac{1 - Y}{Y} \int_0^t \mu(S(\tau))B(\tau). \tag{23}$$

Proposition 4.3. *Fix $X_0^{\mathfrak{u}}$, u and a non-negative initial condition $(X_0^{\mathfrak{s}}, S_0, B_0)$ such that $S_0 < \mu^{-1}(\alpha Y f_1 K_h)$. If $K_d \geq K_h$, there exists $T > 0$ such that for any fixed $t \in [0, T]$, the map $X_0^{\mathfrak{s}} \in \mathbb{R}_+ \mapsto M_t(X_0^{\mathfrak{s}})$ is increasing.*

Proof. Let $X_0^{\mathfrak{u}}$ and $u > 0$, then consider the associated solutions $(X^{\mathfrak{s}}(t), S(t), B(t))$ and $(\bar{X}^{\mathfrak{s}}(t), \bar{S}(t), \bar{B}(t))$ of (19) with initial data $(X_0^{\mathfrak{s}}, S_0, B_0)$ and $(\bar{X}_0^{\mathfrak{s}}, S_0, B_0)$ respectively.
If $\bar{X}_0^{\mathfrak{s}} > X_0^{\mathfrak{s}}$, one can remark that, $Y f_1 K_h (\bar{X}_0^{\mathfrak{s}} - X_0^{\mathfrak{s}}) > 0$, which implies

$$(\bar{X}_0^{\mathfrak{s}}, Z_0, B_0) \succeq (X_0^{\mathfrak{s}}, Z_0, B_0).$$

Furthermore, one gets from (23) and the equations of the model (20)

$$M_t =: M(t) = f_2 \frac{1-Y}{Y}(B(t) - B_0) + K_d \int_0^t B(\tau)d\tau,$$

and

$$\bar{M}_t := \bar{M}(t) = f_2 \frac{1-Y}{Y}(\bar{B}(t) - B_0) + K_d \int_0^t \bar{B}(\tau)d\tau,$$

where $\bar{M}_t, M_t$ are the concentrations of methane produced on the time interval from 0 to t in (20) for the initial conditions $(\bar{X}_0^s, Z_0, B_0)$ and (X_0^s, Z_0, B_0) respectively.
Since

$$K_d \geq K_h \quad \text{and} \quad S_0 < \mu^{-1}(\alpha Y f_1 K_h), \tag{24}$$

the conclusions of Lemma 4.2 guarantee that there exists $T > 0$ such that

$$(\bar{X}^s(t), \bar{Z}(t), \bar{B}(t)) \geq (X^s(t), Z(t), B(t)), \quad \forall t \in [0, T].$$

Therefore,

$$\exists T > 0 : \bar{M}_t > M_t, \quad \forall t \in [0, T].$$

Then, the concentrations of methane $\bar{M}_t$ and M_t produced on the time interval from 0 to t in (19) for the initial conditions $(\bar{X}_0^s, S_0, B_0)$ and (X_0^s, S_0, B_0) respectively, satisfy the same inequality. Thus, the above proposition is proved. ■

Remark 4.4. *In practice, we observe that the conclusion of Proposition 4.3 holds on a large time interval or even over infinite horizon. Consequently, the asymptotic methane production exhibits a monotonic increase with respect to* X_0^s.

5 Numerical computations

The model analysis provided in this paper is valid for all kinetics that satisfy hypothesis $(\mathbf{A_1})$. Non-linear examples of these functions, which are widely used in bioprocesses (see e.g. [31] and Chapter 1.3 of [6]), include Monod [29] and Haldane [3] kinetics, given respectively as follows:

$$\mu(S) = \bar{\mu}\frac{S}{K_s + S} \tag{25}$$

$$\mu(S) = \bar{\mu}\frac{S}{K_s + S + \frac{S^2}{K_i}}, \tag{26}$$

where $\bar{\mu}$, K_s and K_i are positive constants representing, respectively, the maximum growth rate, the half-saturation constant, and the inhibition constant (see Figure 2).

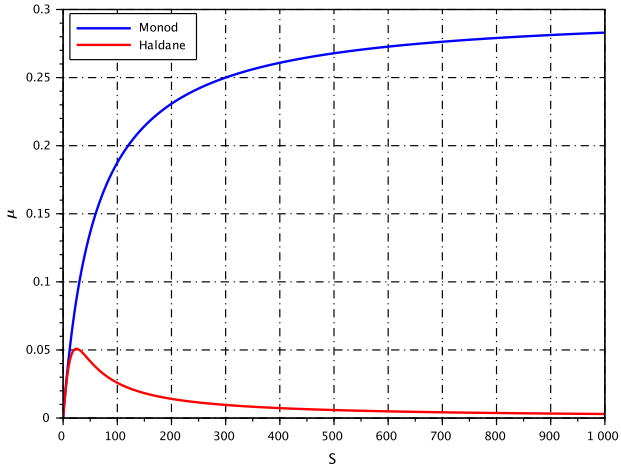

Figure 2: Graphs of Monod and Haldane functions for $\bar{\mu} = 0.3, K_s = 60$ et $K_i = 10$.

To illustrate our approach, we have considered the following numerical simulations for the Monod and Haldane functions, with $\bar{\mu} = 0.3\ h^{-1}$, $K_s = 160\ mg.l^{-1}$ and $K_i = 10\ mg.l^{-1}$ (where h denotes hour). These parameters and other model parameters are borrowed from [40] and reported in Table 2. Moreover, the simple functions

$$\psi(u) = u \qquad \text{and} \qquad g(X^{\mathrm{u}}) = X^{\mathrm{u}}\ (mg.l^{-1})$$

will serve as candidates in our simulations to model the leachate flow rate and the solubilization rate respectively. Specifically, we analyze the impact of initial organic mixing (how the initial matter is distributed in the compartments) and the role of the leachate recirculation rate on methane production.

K_h	K_d	Y	α	f_1	f_2
$0.176\,h^{-1}$	$0.02\,h^{-1}$	0.05	0.9	0.7	0.76

Table 2: Parameters values considered for the numerical simulations.

5.1 Impact of initial condition

Organic biodegradable load is one important parameter influencing performance of anaerobic digestion, since it affects the biogas composition and microbial community. This section investigated the influence of X_0^{s} on methane production in the case of Monod and Haldane response. In particular, numerical sensitivity analyses will be conducted and comparisons will be investigated with the theoretical formula for asymptotic methane production given in Proposition 3.5. The results obtained show that the initial concentration of solubilized organic matter and the leachate parameter u has a significant influence on the degradation of the substrate, production of methane and bacterial population.

Monod kinetics

To illustrate the results provided in section 4.2, we have run numerical simulations for parameters satisfying (24) as it given in Table 3. For Monod kinetics (25), the associated function $\mu^{-1}(.)$ is expressed as follows

$$\mu^{-1}(m) = \frac{K_s m}{\bar{\mu} - m} \quad \text{where} \quad 0 < m < \bar{\mu},$$

then $\mu^{-1}(\alpha Y f_1 K_h) = 98.06$.
We have considered the three initial conditions

$$X_0^1 = (5, 60, 100) \leq X_0^2 = (7, 60, 200) \leq X_0^3 = (7, 61, 300)$$

for $X_0^{\mathrm{u}} = 10$ and $u = 0.1$, where X_0 is the initial condition of (19) in the (X^{s}, S, B)-coordinates. Furthermore, one has

$$H(X_0^1) = 10.35 \leq H(X_0^2) = 10.60 \leq H(X_0^3) = 10.77.$$

K_h	K_d	Y	α	f_1	f_2
$0.176\,h^{-1}$	$0.18\,h^{-1}$	0.9	0.9	0.8	0.76

Table 3: Parameters values considered for the numerical simulations in Figure 3.

Let us notice from Lemma 4.2 that the solutions are ordered in the (X^{s}, Z, B)-coordinates when increasing the initial conditions, but not necessarily in S, where the order of the trajectories is preserved in reverse over the time interval [0,5.5] (see Figure 3 (left)). Even though when increasing X_0^{s} only, the methane production increases as it is illustrated in Figure 3 (right). Since Proposition 4.3 only provides sufficient conditions under which the methane production in (19) increases when increasing initial solubilized organic matter only, the result remains indeed valid even in cases where these conditions are violated but not far to be satisfied. To illustrate this, we choose the initial state as $(X_0^{\mathrm{s}}, S_0, B_0) = (330, 0, 2)$ with a final time $T = 200$, $X_0^{\mathrm{u}} = 30\ mg.l^{-1}$ and an arbitrarily value of $u = 0.01h^{-1}$.

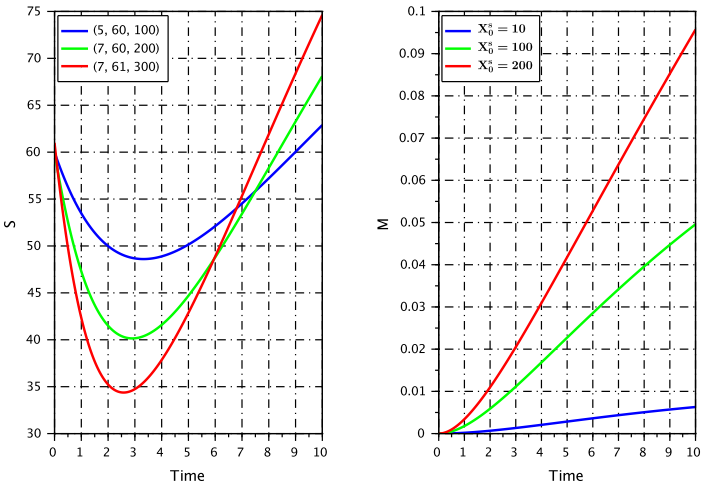

Figure 3: Substrate as a function of time in dynamics (19) for three different initial conditions (left) and methane over time by increasing initial values X_0^s only (right). While the trajectories for substrate concentration cross each other as X_0^s increases, methane production constantly increases as X_0^s increases.

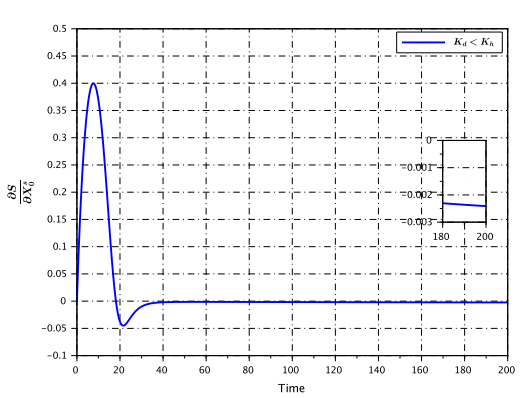

(a) Sensitivity function $\frac{\partial S}{\partial X_0^s}$ with respect to time.

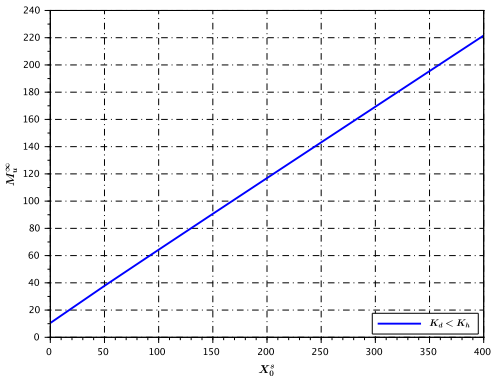

(b) Asymptotic methane production as a function of X_0^s.

Figure 4: The sensitivity function $\frac{\partial S}{\partial X_0^s}$ as a function of time and the asymptotic methane production with respect to the initial value of X_0^s for Monod response with $u = 0.01$. The negative limiting value of $\frac{\partial S}{\partial X_0^s}$ results in an increasing variation of asymptotic methane production with respect to X_0^s.

The values of the parameters used for all subsequent simulations are provided in Table 2. Figure 4a shows the sensitivity of the substrate concentration with respect to the initial solubilized organic matter, $\partial S/\partial X_0^s$, as a function of t when the condition (24) is not fullfilled (for instance $K_d < K_h$). For this case $\partial S/\partial X_0^s$ is positive, increases monotonically in the interval [0,10] and attains its maximum value at $t = 10$ then decreases to attain the minimum at $t = 20$. We note that $t = 30$ is the time when the initial solubilized load affects in a quasi-constant manner the substrate concentration in the system dynamics (19). Furthermore, if we are interested to the asymptotic behavior of the dynamics, one can remark that in this case, the solution converges asymptotically to a very small negative value of -0.0024.

As expected, we remark from the theoretical formula (12) provided in Proposition 3.5 that, if $K_d < K_h$, the limiting value of $\frac{\partial S}{\partial X_0^s}$ is negative which gives a non-negative variation of asymptotic methane with respect to X_0^s. This explains the behavior obtained in Figure 4b: The methane produced asymptotically in (19) is an increasing function of X_0^s for any fixed value of u.

Haldane kinetics

The Haldane law, which models the inhibitory effects at high substrate concentrations, is more suitable for such conditions, compared to the Monod law, which is more appropriate for moderate substrate concentrations. This section focuses on the impact of varying the initial concentration of solubilized matter X_0^s on process performance under different fixed recirculation rates u.
For Haldane kinetics (26), one can check that the set $\mathcal{E}$ has two components

$$\mathcal{E} = [0, \lambda^-] \cup [\lambda^+, +\infty)$$

where

$$\lambda^{\pm} = \frac{\bar{\mu} - K_d \pm \sqrt{\Delta}}{2\frac{K_d}{K_i}}$$

and

$$\Delta = \bar{\mu}^2 - 2\bar{\mu}K_d + \left(1 - 4\frac{K_s}{K_i}\right) K_d^2.$$

The shift in the limiting value S_u^∞ directly impacts the methane production M_u^∞ (as S_u^∞ belongs to the set $\mathcal{E}$) and then the shift in methane production is given by the difference $\frac{\lambda^+ - \lambda^-}{a_1}$ (using the expressions (12) given in Proposition 3.5). Since $\mathcal{E}$ is not connected, the global attractor of system (19) is also non-connected, leading to two attraction basins and then to distinct levels of performance. It can be noted that when $S_0 < \lambda^-$, as long as $S(t) < \lambda^-$, the results concerning increasing kinetics μ apply (Proposition 4.3).

As illustrated in Figure 5, in the absence of recirculation ($u = 0$), for each fixed set of initial conditions X_0^u, S_0 and B_0, the asymptotic value M^∞ (that is M_u^∞ when $u = 0$) undergoes a sudden shift (here approximately 340 units) and shows a discontinuity but the map $u \mapsto M_u^\infty$ is lower semi-continuous as shown in Proposition 4.1.. This is due to the presence of two disjoint connected components in the attractor. Beyond this critical point, denoted as $X_{0,c}^s$, methane production does not reach its maximum potential. Moreover, methane production as a function of X_0^s shows non-monotonic behavior: initially, production increases as long as the equilibrium value of S^∞ (the limiting value of S when $u = 0$) remains below λ^-. However, after reaching a threshold, it starts to decrease when S^∞ exceeds λ^+. The shift value in M^∞ is given by $\frac{\lambda^+ - \lambda^-}{a_1}$, as mentioned earlier. This pattern arises from the inhibitory effects described by the Haldane law, which induces a discontinuity in methane production with respect to X_0^s. Consequently, system performance can be significantly compromised at high initial concentrations of organic matter X_0^s.

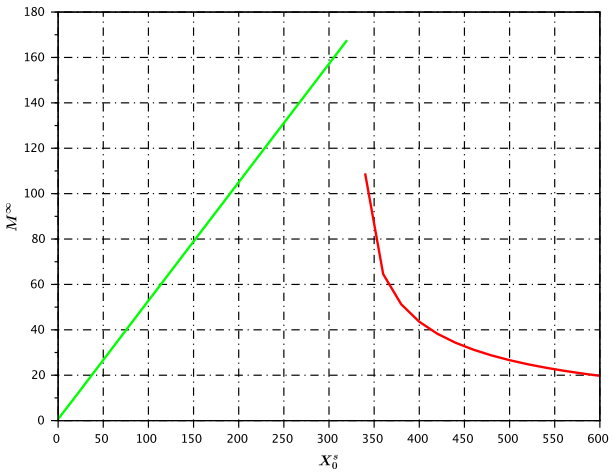

Figure 5: Discontinuity and non-monotonic behavior of methane production as a function of the initial solubilized matter X_0^s without recirculation ($u = 0$) for Haldane kinetics.

For each fixed X_0^u, three feeding scenarios for (19) may arise depending on $X_{0,c}^s$ and the initial organic mixing X_0 (see Figure 6). The plot of $\frac{\partial S}{\partial X_0^s}$ over time for three specific values of u (0, 0.01 and 0.1) shows that this coefficient approaches a positive limit in all cases. According to Proposition 3.5, this limit should be compared with $\frac{f_1}{a_1}$ to evaluate methane production performance.

Case 1: $X_0 < X^{\mathfrak{s}}_{0,c}$ & $X^{\mathfrak{s}}_0 < X^{\mathfrak{s}}_{0,c}$

For $X_0 = 300$, we choose the initial state as $(X^{\mathfrak{s}}_0, S_0, B_0) = (250, 0, 2)$ with a final time $T = 1000$ and $X^{\mathfrak{u}}_0 = 50$. The limiting value of the coefficient $\frac{\partial S}{\partial X^{\mathfrak{s}}_0}$ is less than $\frac{f_1}{a_1}$ (evaluated numerically by 0.52) which gives a positive variation of asymptotic methane with respect to $X^{\mathfrak{s}}_0$. The system exhibits good methane production performance.

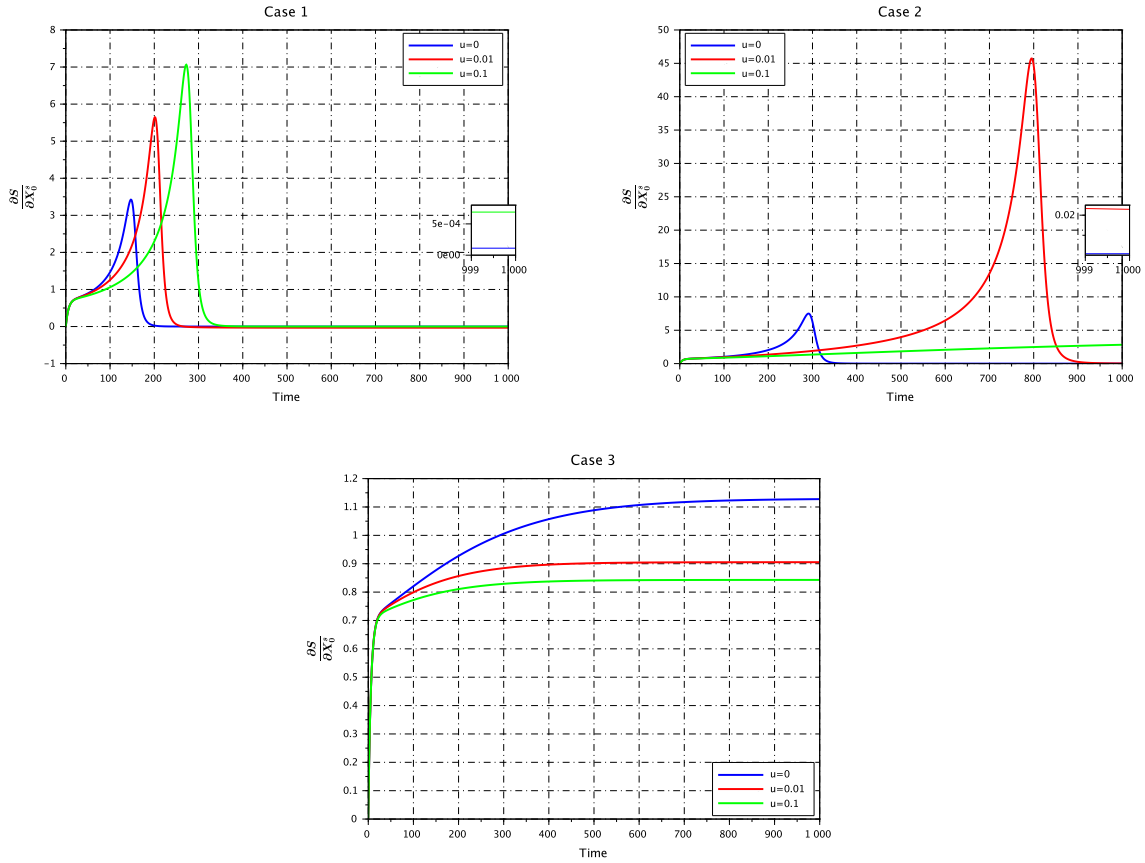

Figure 6: The sensitivity function $\frac{\partial S}{\partial X^{\mathfrak{s}}_0}$ over the time for Haldane response in the three cases for three different values of u between 0 and 0.1. This function approaches a positive limiting value in all cases.

Case 2: $X_0 > X^{\mathfrak{s}}_{0,c}$ & $X^{\mathfrak{s}}_0 < X^{\mathfrak{s}}_{0,c}$

For $X_0 = 360$, we choose the initial state as $(X^{\mathfrak{s}}_0, S_0, B_0) = (300, 0, 2)$ with $X^{\mathfrak{u}}_0 = 60$. Figure 6 (Case 2) suggests that selecting relatively small values of u could maintain the limiting value of the coefficient $\frac{\partial S}{\partial X^{\mathfrak{s}}_0}$ less than $\frac{f_1}{a_1}$. However, there is a risk of lower methane productivity if we slightly miss a determined choice of u. The methane production can be enhanced by choosing a relatively small u and can fall down drastically when the leachate recirculation is relatively large.

Case 3: $X_0 > X^{\mathfrak{s}}_{0,c}$ & $X^{\mathfrak{s}}_0 > X^{\mathfrak{s}}_{0,c}$

For $X_0 = 500$, we choose $X^{\mathfrak{s}}_0 = 400$ with $X^{\mathfrak{u}}_0 = 100$. Since $X^{\mathfrak{s}}_0$ is above the threshold, it is naturally observed that the coefficient significantly exceeds the numerical value of $\frac{f_1}{a_1}$ and thus the performance falls down dramatically.

5.2 Effect of leachate recirculation rate

In this section, we show how methane production is influenced by recirculation rate over time, with a particular focus on the behavior as time approaches infinity. By analyzing the system under both Monod and Haldane growth kinetics, we observe distinct impacts on the methane yield.

Monod kinetics

We first study the time evolution of the methane production, then consider its asymptotic behavior. We can deduce that the influence of leachate recirculation on methane production is significant in the case of Monod kinetics (Figure 7). For instance, the Figure shows that the order of trajectories associated to methane is preserved for the parameter values given in Table 2 and for a range values of recirculation parameter from 0 to 0.1. Let us notice that we took canonical values for initial data ($X_0^s = 300$, $X_0^u = 100, S_0 = 0$ and $B_0 = 2$).

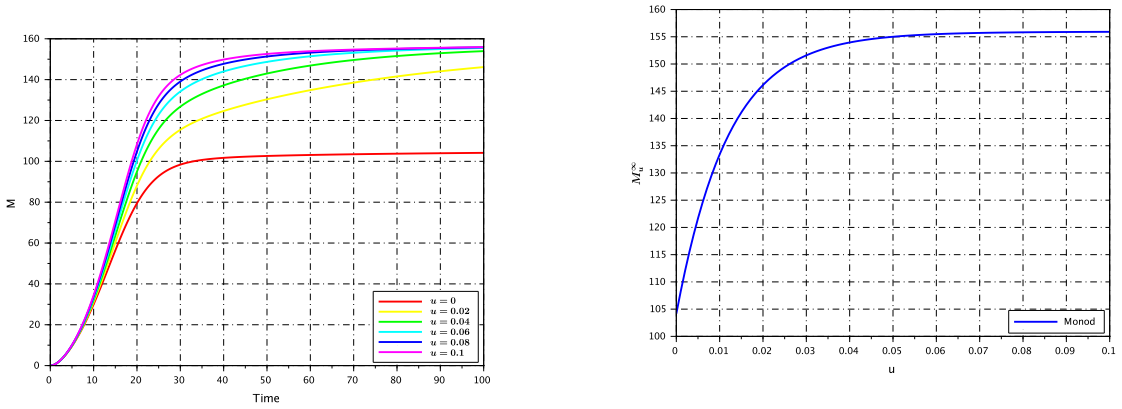

(a) Methane over the time for different values of u.

(b) Effect of recirculation parameter on asymptotic methane prodution.

Figure 7: Behavior of the methane production in dynamics (19) with and without recirculation for Monod kinetics. The order of the trajectories is preserved for a range of recirculation parameter values from 0 to 0.1, leading to an increase in asymptotic methane production as the leachate recirculation parameter u increases.

Figure 7a illustrates that initially the curves show a rapid increase, but as they approach their asymptotic regions, the order among them becomes more pronounced. As expected, the methane produced at a time for which the methane production is close from its asymptotic value is quite high in the case of leachate recirculation ($u > 0$). Thus, we conclude that in the context of Monod kinetics, recirculation enhances methane production. Over time, this leads to an overall increase in methane yield, demonstrating that recirculation is a beneficial strategy for optimizing bioreactor performance under Monod kinetic conditions. Focusing on asymptotic production, the Figure 7b shows that methane production increases with the leachate recirculation parameter u up to approximately 0.05, after which it levels off. The rate of increase slows and eventually saturates beyond this point, indicating that higher values of u do not significantly boost methane production further. Therefore, while increasing u enhances methane output, its effect diminishes after a threshold. To maximize methane production efficiently, it is best to optimize u within this range, as further increases offer minimal additional benefits. This approach can lead to significant cost savings and improved resource efficiency.

Haldane kinetics

When u is large, the recirculation scenario may not significantly impact methane production, suggesting that the simplified model from [40] effectively captures the system's essential dynamics in such cases. However, since our model generalizes the one introduced in [40], it shows that even a small leachate recirculation rate u can affect the asymptotic production on both sides of the switching value of $X_{0,c}^s$.

We first study the time evolution of the methane production. We present the three cases in Figure 8 for

different scenarios of recirculation in the case of Haldane kinetics.

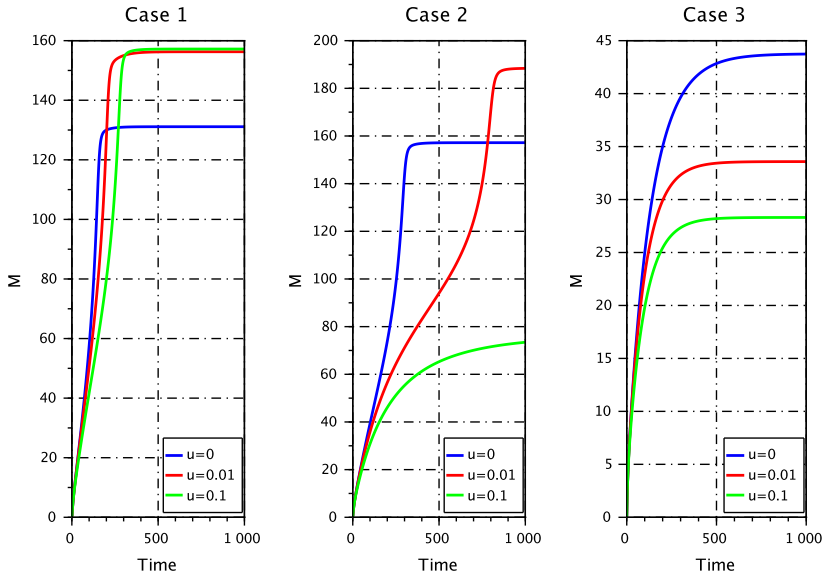

Figure 8: Methane behavior as a function of time in dynamics (19) for different values of u from 0 to 0.1 and for the three cases with Haldane kinetics . While methane production continues to increase over time, the production curves are not ordered with respect to u.

Case 1: $X_0 < X^{s}_{0,c}$ & $X^{s}_0 < X^{s}_{0,c}$

We choose the initial state as $(X^{s}_0, S_0, B_0) = (250, 0, 2)$ with a final time $T = 1000$ and $X^{u}_0 = 50$. In Figure 8 (Case 1), the methane production behavior is shown for three different values of the recirculation parameter $u : 0, 0.01$; and 0.1. The plot indicates that the methane production reaches a high asymptotic value about 160 units regardless of the recirculation rate. The curves for $u = 0$ and $u = 0.01$ converge quickly to this asymptotic value, while for $u = 0.1$, the convergence is slightly slower but still reaches the same asymptotic value. This suggests that in Case 1, recirculation has a minimal impact on the final methane production, indicating a final methane production which is robust with respect to the recirculation rate u.

Case 2: $X_0 > X^{s}_{0,c}$ & $X^{s}_0 < X^{s}_{0,c}$

In this case, we choose $X^{s}_0 = 300$ with $X^{u}_0 = 60$. As it is seen in Figure 8 (Case 2), the methane production shows more variability with different recirculation rates. For $u = 0$ (blue curve), methane production reaches an asymptotic value about 160 units, similar to Case 1. For $u = 0.01$, when increasing slightly the value of u, the asymptotic value of methane increases. However, for $u = 0.1$ (green curve), the asymptotic value is lower, resulting in the lowest production level. This indicates that higher recirculation rates negatively impact methane production in this scenario, due to inhibitory effects and suboptimal conditions. According to the considered case, since we start with an initial solubilized matter less than the critical value $X^{s}_{0,c}$, it is important to carefully choose the recirculation rate u that ensures the solubilization of X^{u} without accumulating in a way that exceeds the critical threshold $X^{s}_{0,c}$. This behaviour can be explained by the existence of an optimal u that achieves a solubilization of X^{u} such that we remain in the left interval of the attractor (Case 1).

Case 3: $X_0 > X^{s}_{0,c}$ & $X^{s}_0 > X^{s}_{0,c}$

Here, we choose $X^{s}_0 = 400$ with $X^{u}_0 = 100$. In the third case of Figure 8, the impact of recirculation on methane production is even more pronounced. For $u = 0$ (blue curve), the methane production reaches an asymptotic value about 43 units. As the recirculation rate increases to $u = 0.01$ (red curve) and $u = 0.1$ (green curve), the asymptotic values decrease significantly, up to $u = 0.1$ producing the lowest amount of methane. This trend indicates that higher recirculation rates adversely affect methane production in Case 3, suggesting that the

system might be highly sensitive to recirculation, due to substrate inhibition at higher recirculation rates. Thus, an unavoidable scenario of poor methane productivity emerges.

In the case of Monod kinetics, recirculation tends to enhance methane production (Figure 7), but in Haldane kinetics, which considers substrate inhibition at high concentrations, the interaction is more complex. While methane production continues to increase over time, the production curves are not ordered with respect to u and can even intersect, as illustrated in Figure 8. These differences highlight the critical role of recirculation in optimizing methane production in bioreactors, emphasizing the need to tailor recirculation strategies according to the specific growth kinetics of the microbial community involved.

To illustrate the results provided in Subsection 4.1.2 (large recirculation rates), we present a numerical comparison between the methane production of system (15) and the reduced model (17) (Figure 9). We choose the initial state and the final time for each feeding scenario as presented in Figure 8, with a value of $u = 0.1$.

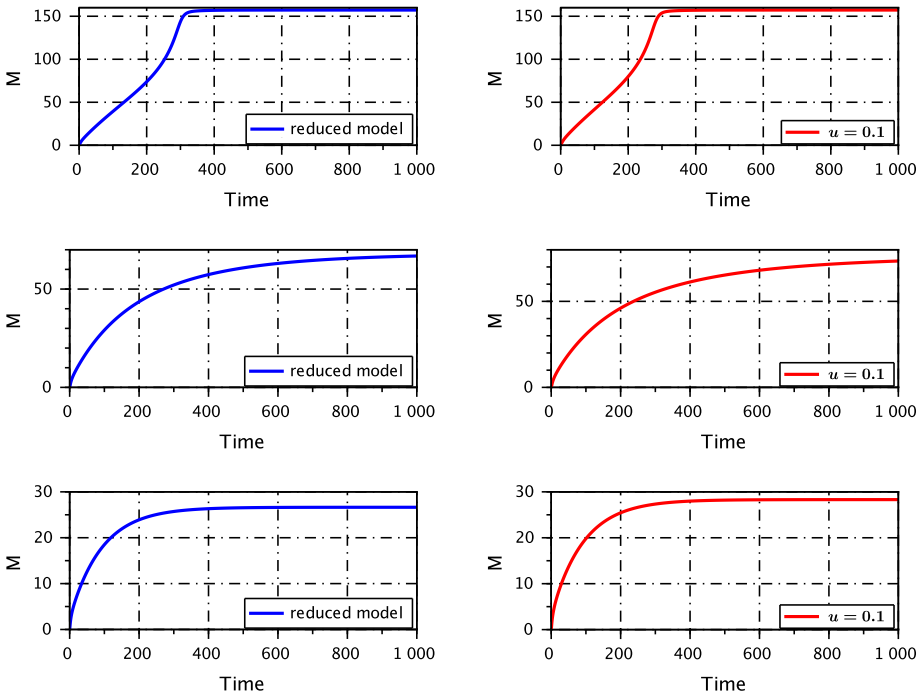

Figure 9: Comparison of methane production with the dynamics (17) (left) and (15) (right) for u relatively large under Haldane kinetics in the three cases. When the recirculation parameter is high, the difference in methane production between the two models becomes negligible.

For the three feeding scenarios, there is no significant difference in methane yield between the models (17) and (15) when recirculation is very large. For instance, the asymptotic values of methane produced in systems (17) and (15) are about 67 units and 73 units, respectively for the second scenario of feeding (see Figure 9), indicating that the difference between these values is on the order of $1/u$. In most cases, the solubilization of X^{u} occurs rapidly. Therefore, when the recirculation parameter is high, the difference in methane production between the two models becomes negligible. This suggests that the impact of recirculation is minimal in this context, as the dynamics with the absence of recirculation (introduced in [40]) closely approximates the behavior of the generalized model (1) under high recirculation conditions. Thus, the impact of recirculation is more notably observed for small values of u.

Finally, we highlight the influence of the leachate recirculation on the asymptotic methane production for the Haldane response in the three cases. We keep all parameters the same as in Figure 8 and plot the curve of methane production as a function of the recirculation rate u. We keep the following bounds on the parameter $u_{min} = 0$ and $u_{max} = 0.1$.

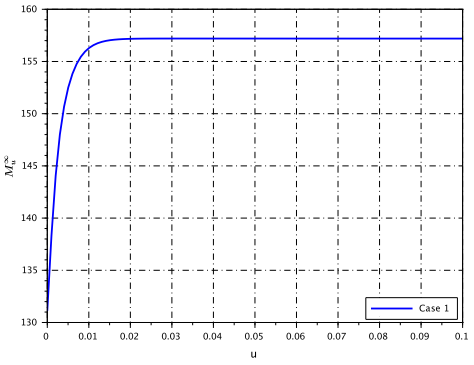

(a) For $X_0^s = 250$

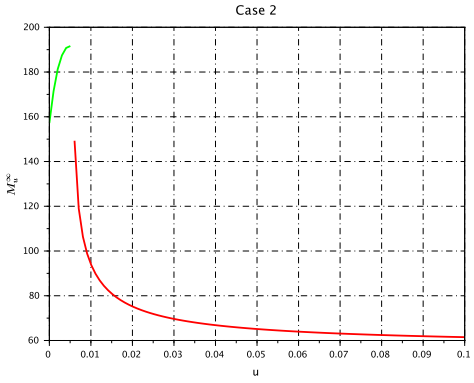

(b) For $X_0^s = 300$

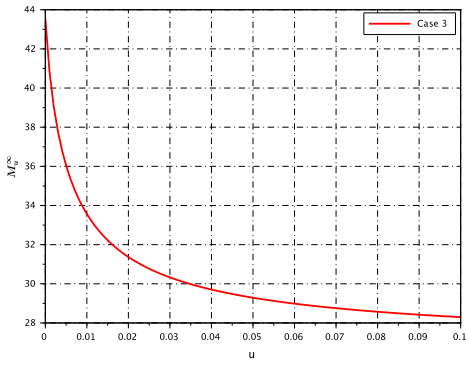

(c) For $X_0^s = 400$

Figure 10: The impact of recirculation rate on asymptotic methane production for three different initial substrate concentrations with Haldane kinetics.

In Case 1, methane production in Figure 10 (a) shows a positive response to increasing recirculation rate. As u increases from 0 to 0.1, the asymptotic methane production (M_u^∞) also increases, up to 155-160 units. This indicates that in this scenario, higher recirculation rates enhance methane production.
Case 2 represented by Figure 10 (b), shows a different trend. Initially, for very low recirculation rates (up to approximately u=0.01), methane production is high and remains close to 200 units. However, as the recirculation rate increases beyond this point, there is a significant decrease in methane production, dropping to about 60 units at u=0.1. This suggests that while a small amount of recirculation can be beneficial, higher rates lead to diminished methane yields, potentially due to substrate inhibition.
In Figure 10 (c), the effect of recirculation on methane production is negative. As the recirculation rate u increases from 0 to 0.1, the asymptotic methane production decreases steadily from about 44 units to approximately 28 units. This trend indicates that higher recirculation rates systematically reduce methane production in this case, due to inhibition and high concentrations of substrate created by high recirculation.

To summarize, as seen in Figure 10, the figures illustrate the impact of recirculation rate on methane production for different initial substrate concentrations. In Case 1, increasing recirculation enhances methane production, while in Case 2, there is an optimal low recirculation rate beyond which production declines. In Case 3, any further increase in recirculation rate results in a decrease in methane production, making the no-recirculation scenario the most effective. These observations emphasize the importance of choosing recirculation rates accordingly to the specific system dynamics and initial conditions to obtain a good methane production.

5.3 Effect of both initial condition and leachate recirculation on methane production

This subsection offers a global visualization of how methane production is affected by both variations of the initial unsolubilized matter X_0^{u} and the recirculation parameter u for Haldane kinetics. As shown in Figure 11,

the parameter u strongly inhibits methane production, and thus keeping u low is crucial for maximizing methane output.
The 3D plot allows us to draw the following observations:

- **General trend:** The graph shows a lowering surface as u increases, indicating that methane production decreases with increasing u. When u is near to zero, the methane production is higher, especially for lower values of X_0^{u}.
- **Behavior at low u:** At low values of u (near 0), the methane production is maximized when X_0^{u} is also low. As X_0^{u} increases, the methane production decreases gradually even at low u.
- **Behavior at high u:** At high values of u, the methane production is significantly lower for all values of X_0^{u}. The surface becomes almost flat at higher u, indicating an inhibitory effect.
- **Optimal regions:** The highest methane production is observed at low u and low X_0^{u}, presenting a peak. As either u or X_0^{u} increases, methane production drops, showing a valley.

Finally, we conclude that the combined effect of u and X_0^{u} suggests a non-linear interaction where both parameters should be chosen together for the best methane production.

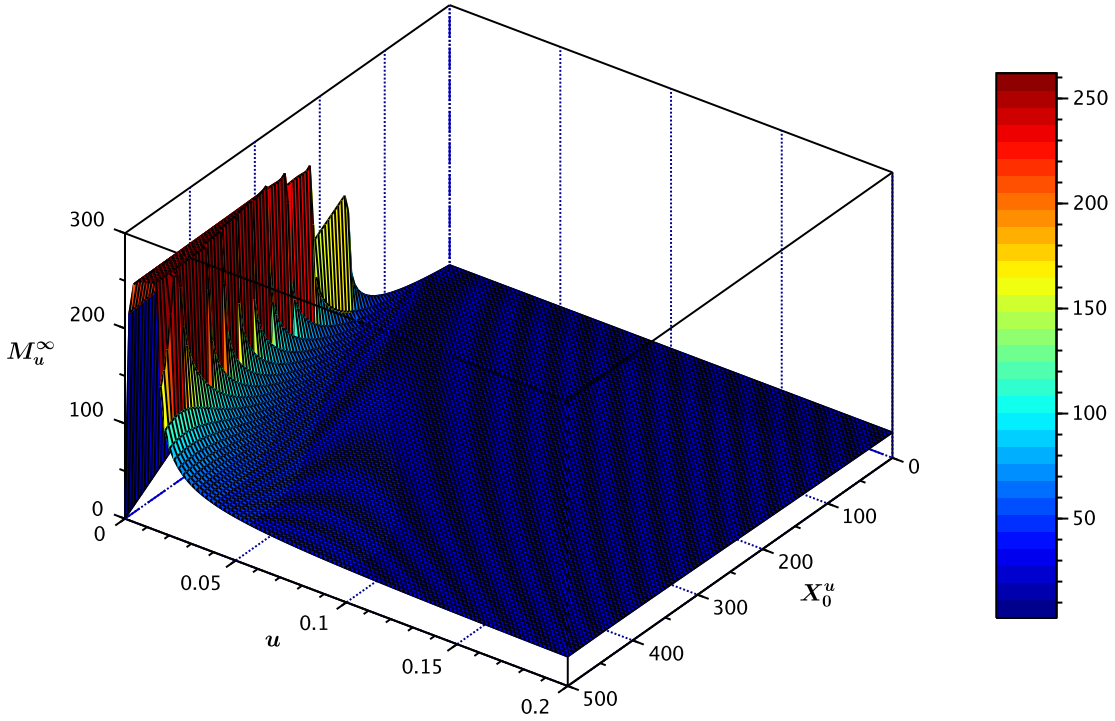

Figure 11: Methane production as a function of initial unsolubilized matter and leachate recirculation rate for Haldane kinetics (3D plot).

6 Conclusion and perspectives

We have studied a five-dimensional, two-step anaerobic digestion system under perfect organic mixing considering the presence of unsolubilized organic matter. Taking into account the leachate recirculation, we have considered two components: the first is unsolubilized matter, which undergoes a solubilization process, transforming into the second component—solubilized matter that is converted by methanogenic bacteria to produce the methane. Our model is general, encompassing a broader range of dynamics compared to previous formulations. In particular, the

model proposed in [40] appears as a specific case of our framework, as it considers only solubilized organic matter and neglects recirculation. This extension allows a more comprehensive representation of the digestion process, providing deeper insights into the interplay between solubilization dynamics, microbial activity, and methane production. We have taken benefit of a partial cascade structure of this model to analyze the global behavior of the system and estimate the theoretical methane output. Furthermore, we studied the asymptotic behavior of the solutions and characterized its global attractor composed of non-hyperbolic equilibria. By demonstrating how a partial order of the solutions can be preserved under monotonic growth conditions, we have provided insights into the impact of recirculation rate on system behavior.

The mathematical analysis of the problem was followed by numerical simulations. We have investigated the sensitivity of the residual substrate with respect to the initial organic loading X_0. Our primary objective was to focus on the total methane production and measure sensitivity for Monod or Haldane kinetics. Depending on the proportion of unsolubilized matter within the total initial organic matter and in the presence of substrate inhibition, our numerical results reveal a range of possible operational scenarios, from organic matter underfeeding, causing an average production of methane, to organic matter overfeeding, leading to a poor methane production. Additionally, we identified conditions where a minimum level of recirculation enhances gas production, offering valuable guidance for optimizing anaerobic digestion processes.

Beyond its mathematical contributions, this work has significant implications for the optimization of biogas production in real situations. Through our analysis, particularly regarding the value of asymptotic methane production under the combined effect of recirculation and organic distribution using a 3D representation, we have drawn key insights for practitioners about the effect of recirculation on methane production in biodegradation processes under different initial conditions and growth kinetics. An interesting perspective would be to consider a time-dependent recirculation rate and to determine an optimal strategy for leachate recirculation in order to maximize the methane production in the presence of an inhibition phenomenon. Since multiple cost sources come into play in the solubilization process, it would also be more realistic to consider maximizing gas production while accounting for recirculation operation costs. The study of the optimal recirculation strategy constitutes an interesting challenge. Beyond optimizing recirculation, future research could focus on extending the model to account for additional microbial interactions, variable environmental conditions, or stochastic perturbations. Additionally, it would be relevant to take into account the spatial distribution of matter inside the landfill and investigate reaction-diffusion models in terms of systems of partial differential equation systems. Finally, experimental validation of our theoretical predictions would help refine the model and enhance its applicability to real-world digestion systems.

Acknowledgments

The authors thank the French Embassy in Morocco and the TSARA program of INRAE for funding the first author's visits to France during the preparation of her PhD. We also express our gratitude to the referees for their insightful comments, which have significantly contributed to improving the paper.

References

[1] O. H. Abdelkader, A. H. Abdelkader, Modeling Anaerobic Digestion Using Stochastic Approaches, in Trends in Biomathematics: Mathematical Modeling for Health, Harvesting, and Population Dynamics, Springer International Publishing, vol. 99, pp. 373–396, 2019.

[2] H. H. Almuashi, N. A. Almuallem, and M. El Hajji, The effect of leachate recycling on the dynamics of two competing bacteria with an obligate one-way beneficial relationship in a chemostat, Mathematics, vol. 12, p. 3819, 2024.

[3] J. Andrews, A mathematical model for the continuous culture of microorganisms utilizing inhibitory substrates, Biotechnology and Bioengineering, vol. 10, no. 6, pp. 707–723, 1968.

[4] I. Barbalat, Systèmes d'équations différentielles d'oscillations non linéaires, Revue Mathématiques Pures et Appliquées, vol. 4, pp. 267–270, 1959.

[5] M. A. Barlaz, J. P. Chanton, R. B. Green, Controls on landfill gas collection efficiency: instantaneous and lifetime performance, Journal of the Air & Waste Management Association, vol. 59, no. 12, pp. 1399–1404, 2009.

[6] G. Bastin and D. Dochain, On-line Estimation and Adaptive Control of Bioreactors, Elsevier, Amsterdam, 1990.

[7] D. J. Batstone, J. Keller, I. Angelidaki, S. V. Kalyuzhnyi, S. G. Pavlostathis, A. Rozzi, W. T. M. Sanders, H. Siegrist, V. A. Vavilin, The IWA anaerobic digestion model no 1 (ADM1), Water Science and Technology, vol. 45, pp. 65–73, 2002.

[8] D. J. Batstone, D. Puyol, X. Flores-Alsina, J. Rodríguez, Mathematical modelling of anaerobic digestion processes: Applications and future needs, Reviews in Environmental Science and Biotechnology, vol. 14, pp. 595–613, 2015.

[9] H. Benbelkacem, R. Bayard, A. Abdelhay et al., Effect of leachate injection modes on municipal solid waste degradation in anaerobic bioreactor, Bioresource Technology, vol. 101, no. 14, pp. 5206–5212, 2010.

[10] O. Bernard, Z. Hadj Sadock, D. Dochain, A. Genovesi, J. P. Steyer, Dynamical model development and parameter identification for an anaerobic wastewater treatment process, Biotechnology and Bioengineering, vol. 75, no. 4, pp. 424–438, 2001.

[11] M. S. Bilgili, A. Demir, G. Varank, Evaluation and modeling of biochemical methane potential (BMP) of landfilled solid waste: a pilot scale study, Bioresource Technology, vol. 100, no. 12, pp. 4976–4980, 2009.

[12] S. Bozkurt, L. Moreno, I. Neretnieks, Long-term processes in waste deposits, Science of the Total Environment, vol. 250, no. 1–3, pp. 101–121, 2000.

[13] L. N. H. Chen, Anaerobic Digestion Basics, University of Idaho Extension, Moscow, ID, USA, 2014.

[14] D. Chenu, Modélisation des transferts réactifs de masse et de chaleur dans les installations de stockage de déchets ménagers: application aux installations de type bioréacteur, PhD thesis, Institut National Polytechnique de Toulouse, France, 2007.

[15] A. Colantoni, M. Carlini, E. Mosconi, S. Castellucci, M. Villarini, An Economical Evaluation of Anaerobic Digestion Plants Fed with Organic Agro-Industrial Waste, Energies, vol. 10, no. 8, pp. 1165, 2017.

[16] M. El Hajji, Mathematical modeling for anaerobic digestion under the influence of leachate recirculation, AIMS Mathematics, vol. 8, no. 12, pp. 30287–30312, 2023.

[17] M. El Hajji, Influence of the presence of a pathogen and leachate recirculation on a bacterial competition, International Journal of Biomathematics, online ready, p. 2450029, 2024.

[18] M. El Hajji, F. Mazenc, J. Harmand, A mathematical study of syntrophic relationship of a model of anaerobic digestion process, Mathematical Biosciences and Engineering, vol. 7, no. 3, pp. 641–656, 2010.

[19] J. Harmand, A. Rapaport, N. Dimitrova, I. Simeonov, Modelling and Optimal Design of Complex Biological Systems, Processes, vol. 11, no. 1, pp. 105, 2023.

[20] J. Hess, O. Bernard, Design and study of a risk management criterion for an unstable wastewater treatment process, Journal of Process Control, vol. 18, no. 1, pp. 71–79, 2008.

[21] M. Hirsch, Systems of differential equations which are competitive or cooperative I. Limit sets, SIAM Journal on Mathematical Analysis, vol. 13, no. 2, pp. 167–179, 1982.

[22] S. Jeyaseelan, A simple mathematical model for anaerobic digestion process, Water Science and Technology, vol. 35, no. 8, pp. 185–191, 1997.

[23] J. Jiang, G. Yang, Z. Deng et al., Pilot-scale experiment on anaerobic bioreactor landfills in China, Waste Management, vol. 27, no. 7, pp. 893–901, 2007.

[24] H. K. Khalil, Nonlinear Systems, 2nd Edition, Prentice-Hall, New York, 1996.

[25] L. Lardon, J. P. Steyer, Advances in Diagnosis of Biological Anaerobic Wastewater Treatment Plants, Lecture Notes in Control and Information Sciences, vol. 361, pp. 285–311, Springer, Berlin/Heidelberg, 2007.

[26] J. Mabrouki, Mathematical Modelling of Biogas Production in a Controlled Landfill: Characterization, Valorization Study and Energy Potential, Sustainability, vol. 14, no. 23, pp. 1–15, 2022.

[27] J. Mataalvarez, S. Mace, P. Llabres, Anaerobic digestion of organic solid wastes–an overview of research achievements and perspectives, Bioresource Technology, vol. 74, no. 1, pp. 3–16, 2000.

[28] A. Mazur, How does population growth contribute to rising energy consumption in America?, Population and Environment, vol. 15, no. 5, pp. 371–378, 1994.

[29] J. Monod, La technique de la culture continue: Théorie et applications, Annales de l'Institut Pasteur, vol. 79, pp. 390–410, 1950.

[30] J. Pacey, D. Augenstein, R. Morck, D. Reinhart, R. Yazdani, The bioreactor landfill - An innovation in solid waste management, MSW Management, 1999.

[31] S. G. Pavlostathis, E. Giraldo-Gomez, Kinetics of anaerobic treatment : a critical review, Critical Reviews in Environmental Control, vol. 21, pp. 411-490, 1991.

[32] L. Perko, Differential Equations and Dynamical Systems, Springer, 3rd edition, 2011.

[33] F. G. Pohland, Leachate recycle as landfill management option, Journal of the Environmental Engineering Division, ASCE, vol. 106, no. 5, pp. 1057–1069, 1980.

[34] G. E. Powell, Stable coexistence of syntrophic associations in continuous culture, Journal of Chemical Technology and Biotechnology, vol. 35, no. 1, pp. 46–50, 1985.

[35] A. Ramachandran, R. Rustum, A. J. Adeloye, Review of Anaerobic Digestion Modeling and Optimization Using Nature-Inspired Techniques, Processes, vol. 7, no. 12, pp. 953, 2019.

[36] A. Rapaport, T. Bayen, M. Sebbah, A. Donoso-Bravo, A. Torrico, Dynamical modelling and optimal control of landfills, Mathematical Methods and Models in Applied Sciences (M3AS), vol. 26, no. 3, pp. 901–929, 2016.

[37] A. Rapaport, O. Laraj, N. El Khattabi, Comparison of solutions for non-monotone dynamical systems, Systems & Control Letters, vol. 191, no. 105862, 2024.

[38] D. Reinhart, A. B. Al-Yousfi, The impact of leachate recirculation on municipal solid waste landfill operating characteristics, Waste Management and Research, vol. 14, no. 4, pp. 337–346, 1996.

[39] M. Rouez, Dégradation anaérobie de déchets solides: Caractérisation, facteurs d'influence et modélisations, PhD thesis, Institut National des Sciences Appliquées, Lyon, France, 2008.

[40] S. Ouchtout, Z. Mghazli, J. Harmand, A. Rapaport, Z. Belhachmi, Analysis of an anaerobic digestion model in landfill with mortality term, Communications in Pure and Applied Analysis, vol. 19, no. 4, pp. 2333–2346, 2020.

[41] T. M. Sandipa, C. K. Kanchana, H. B. Ashok, Enhancement of methane production and bio-stabilisation of municipal solid waste in anaerobic bioreactor landfill, Bioresource Technology, vol. 110, pp. 10–17, 2012.

[42] D. T. Sponza, O. N. Agdag, Impact of leachate recirculation and recirculation volume on stabilization of municipal solid wastes in simulated anaerobic bioreactors, Process Biochemistry, vol. 39, no. 11, pp. 2157–2165, 2004.

[43] M. Vidyasagar, Nonlinear Systems Analysis, Society for Industrial and Applied Mathematics, 2002.

[44] S. Walcher, On cooperative systems with respect to arbitrary orderings, Journal of Mathematical Analysis and Applications, vol. 263, no. 2, pp. 543–554, 2001.

[45] W. Walter, Ordinary Differential Equations, Springer, 1998.

[46] M. Warith, Bioreactor landfills: experimental and field results, Waste Management, vol. 22, no. 1, pp. 7–17, 2002.